Connected Vehicles Using Visible Light Communications and Dedicated Short-Range Communications

CONNECTED VEHICLES USING VISIBLE LIGHT COMMUNICATIONS AND DEDICATED SHORT-RANGE COMMUNICATIONS

BY

AHMED DARWISH, B.Sc.

A THESIS

SUBMITTED TO THE DEPARTMENT OF ELECTRICAL & COMPUTER ENGINEERING

AND THE SCHOOL OF GRADUATE STUDIES

OF MCMASTER UNIVERSITY

IN PARTIAL FULFILMENT OF THE REQUIREMENTS

FOR THE DEGREE OF

MASTER OF APPLIED SCIENCE

Master of Applied Science (2016) McMaster University

(Electrical & Computer Engineering) Hamilton, Ontario, Canada

TITLE: Connected Vehicles Using Visible Light Communications and Dedicated Short-Range Communications

AUTHOR: Ahmed Darwish

B.Sc., (Electronics and Communications Engineering)

Cairo University, Cairo, Egypt

SUPERVISOR: Dr. Steve Hranilovic

NUMBER OF PAGES: xv, 118

To my parents

Abstract

Connected Vehicle (CV) is a motorized vehicle that can communicate with its interior and exterior surroundings. Connected Vehicle focuses on localized vehicle-to-vehicle (V2V) and vehicle-to-infrastructure (V2I) to support safety, mobility and environmental applications.

In this work, a simulation framework is presented. The framework quantifies Connected Vehicle performance in a forward collision warning situation. The simulation framework evaluates the performance using a vehicular traffic simulator with data from an intersection in Toronto, ON Canada. Various communication methodologies are evaluated at different Connected Vehicle market penetration rates. While DSRC is an interference limited communication methodology and visible light communications is a line-of-sight communication, the combination of both is evaluated to quantify the vehicular network safety performance in terms of time to collision. The performance of DSRC in a vehicular network is quantified in an interference dominant environment and the VLC performance in the vehicular network is evaluated at different weather conditions. In a specific vehicular traffic situation namely forward collision warning, this research quantified the VLC performance improvement in vehicular network safety to be 11% in addition to DSRC.

This work concludes with the simulation and prototyping of camera communications for vehicular applications. Specifically this thesis presents multiple input / multiple output camera communications link utilizing a luminary array as a transmitter and two orthogonal low cost rolling shutter cameras as a receiver with the purpose of increasing the achievable data rate with one camera.

This work has demonstrated that there is at most a doubling in the data rate using two cameras over a single one. This data rate increase is achievable using a specific camera setup namely orthogonal cameras.

Acknowledgements

All the praises and thanks be to God, the Most Merciful, the Most Compassionate.

I would like to thank Dr. Steve Hranilovic for his guidance and mentorship throughout my graduate career. Dr Steve is an excellent mentor not only on the professional level but also on the personal level.

I would like also to thank Dr. Saiedeh Razavi and her student Wade Genders from McMaster Civil Engineering Department for their collaboration to produce the vehicle traffic statistics in Chapter 3 and Chapter 4.

Special thanks for Prof. Zabih (Fary) Ghassemlooy, and Oliver Luo from Northumbria University, UK for their constructive discussion in visible light communication model development (Chapter 4). This work wont be possible without the technical aid of Warren Pawlikowski and valuable discussions with my colleagues Mohamed Salah, Michel Taylor, Lu Min, Eric Edwards, Dingchen Zhang and Boxiao Han.

Acronyms

AWGN	Additive White Gaussian Noise
BER	Bit Error Rate
CamComm	Camera Communication
CCH	Control Channel
CDF	Cumulative Distribution Function
CDMA	Code Division Multiple Access
DOT	Department of Transportation
DSRC	Dedicated Short-Range Communications
ECU	Electronic Control Unit
FCC	Federal Communications Commission
FCW	Forward Collision Warning
FDMA	Frequency Division Multiple Access
GF	Galois Field
GPS	Global Positioning System
IEEE	Institute of Electrical and Electronics Engineers
ITS	Intelligent Transportation System
JEITA	Japan Electronics and Information Technology Industries Association
LED	Light Emitting Diode

LOS	Line-Of-Sight
MAC	Media Access Control Layer
MIMO	Multiple Input Multiple Output
NHTSA	National Highway Traffic Safety Administration
NLOS	Non-Line-Of-Sight
OBD	On-Board Diagnostics
OFDM	Orthogonal Frequency Division Multiplexing
OMEGA	project hOME Gigabit Access
PAM	Pulse Amplitude Modulation
PDF	Probability Density Function
PDP	Power Delay Profile
PDR	Packet Delivery Ratio
PHY	Physical Layer
RFID	Radio-Frequency Identification
RGB	Red Green Blue
SCH	Service Channel
TDMA	Time Division Multiple Access
TTC	Time to Collision
UFSOOK	Undersampled Frequency Shift ON-OFF Keying
US	United States
V2V	Vehicle to Vehicle
VLC	Visible Light Communication
VLCC	Visible Light Communications Consortium
WHO	World Health Organization

Contents

List of Figures

List of Tables

Chapter 1

Introduction

According to the World Health Organization (WHO), every year from 2004 to 2009 1.2 million people lost their lives in traffic accidents and $20 - 50$ million suffer from serious traffic related injuries world wide. In the same study, more people in the age group $15 - 29$ die from traffic accidents than HIV/AIDs [11]. A different study [12] projects an increase in road traffic accidents death to reach 2.1 million in 2030.

Since the second industrial revolution in the 19th century with the first gasoline vehicle manufactured in 1886, motor vehicles have not stopped evolving. Multiple sensors can be found in modern day cars. For example driver fatigue detection sensor, tire pressure sensor and wheel speed sensor. An exhaustive list of automotive sensors is presented in [13]. A recent study [14] expects that the number of sensors in the car will rise from the current average of 60 - 100 sensors to 200 sensors by 2020.

The term *Connected Vehicle* (CV) is used interchangeably in the literature as intra-vehicle connectivity or inter-vehicle connectivity. In this thesis, *Connected Vehicle* is defined as a motorized vehicle that can communicate with its external surroundings, to other CVs, or to infrastructure. The term Connected Vehicle can be

used for a broad range of vehicles starting with a vehicle that can perform simple driver assistant task up to a fully autonomous vehicle.

CVs have the potential to positively impact tens of millions of people. The Google Self-Driving car has driven $1,268,108$ miles in the autonomous mode [15]. Since the start of the project in 2009 until October 2015 Google Self-Driving car had 12 minor accidents and the self driving car was never the cause of the accident [15]. The Google self driving car uses radar sensors, cameras and lasers to perform autonomously and detect objects in all directions.

Automobile manufactures started to implement separate features that will assist the driver and they are a step closer to the fully autonomous car namely lane departure warning, parking assistant, traffic jam assistant and lane control assistant. Volvo promised its customers 100 autonomous vehicles by 2017 [16]. On October, 2015 Toyota announced a car that can drive independently from the highway entrance to the exit [17]. In the same month Tesla Motors announced auto pilot software update as an incremental improvement to self-driving technology utilizing pre-installed 12 long-range ultrasonic sensors, forward radar and forward looking camera [18].

Moreover, government mandates on CVs have expedited its deployment. The European Commission proposed to implement an *eCall system* in cars by April 2018. In such a system, cars will be able to automatically establish a telephone link in case of emergency, such as in a collision [19]. Similarly General Motors developed a similar system named OnStar, in this system there is a emergency automatic crash response [20].

In the United States (US), the Department of Transportation (DOT) and National Highway Traffic Safety Administration (NHTSA) announced a mandate for

car manufacturers to enable car communication for light vehicles, the agency believes that having such mandate will facilitate development of vehicle safety applications for example to reduce intersection crashes which are the deadliest among the US drivers [21].

Also the US states of Nevada, California, Michigan, North Dakota, Tennessee and Florida have passed laws to permit testing autonomous vehicles on public roads [22]. In Canada, starting January 2016 Ontario allowed self-driving cars for testing on public roads [23].

Intelligent Transportation Systems (ITS) are applications that utilize information and communication technologies to inform users and to allow them to coordinate the use of transport network (e.g. traffic signal control, intelligent traffic scheduling and fleet management). CVs cooperate and coordinate together to enable different applications for road safety (e.g., lane departure warning when the vehicle starts to leave its lane, and cooperative lane merging by informing vehicles in range during the lane change process) thus it is an enabler technology for ITS [24].

Equipping CVs with wireless connectivity will improve safety on the road. CVs aim to avoid the accident before it happens. Avoiding accidents is the best way to eliminate injuries and fatalities thus make the roads safer [25],[26].

CVs promise to improve traffic management [27]. There are multiple causes for today's traffic congestion namely accidents, construction work, weather conditions and increases in traffic volume. Traffic congestion results in environmental as well as economic losses [28]. CV promises traffic management improvement in terms of trip time. In [29], researchers have found vehicle speed increase from 67 km/h to 88 km/h in a traffic queue of 60 vehicles in 2000 meters utilizing a congestion control

algorithm.

The percentage of CVs traveling on the road is predicted to increase from 10% to 90% by 2020 [30]. Various research institutions are working on achieving this goal, for example in [31], the authors developed a WiFi enabled vehicle that communicate with multiple stations simultaneously exploiting basestation diversity to eliminate disruptions due to handoff in a network of 10 WiFi stations and using 40 km/h speed vehicle.

An online vehicle diagnostic system is presented in [32], where the location of the vehicle is obtained through GPS (Global Positioning System). The engine information is interfaced using the vehicle on-board diagnostic (OBD), this real time data is transmitted on 3G network.

CVs share their sensor information [33] (e.g., speed and acceleration sensors) with other Connected Vehicles in it is proximity as well as CVs which are multiple hops away to create a small ad hoc network without the need of infrastructure [14]. The shared information informs the CV with any possible "unsafe" situation for example vehicle running red light, thus improve road safety by utilizing different applications such as collision detection and lane changing.

Securing the CV shared information is crucial [34],[35]. Research has shown the ability to relay radio signal from the vehicle key to the vehicle itself without compromising its security [36]. Others managed to access tire pressure monitoring system to set false low tire pressure warning [37]. Two hackers spent one year working on hacking Jeep SUV they managed to remotely shutdown the engine while the car is being driven on the highway [38].

CVs have been a focus for the research industry for a long time [39], mainly how

to establish a reliable wireless communication link between vehicles [40]. One of the CV challenge is to overcome the communication environment in urban situations where a line-of-sight (LOS) link doesn't always exist [41]. Accurate modeling of the propagation channel environment is vital to be able to design a reliable vehicular communication system.

In the next sections of this chapter the suggested communication technologies for the *Connected Vehicle* application (DSRC-VLC-CamComm) are introduced. Finally, this chapter concludes with the thesis organization and contributions.

1.1 Dedicated Short Range Communications

Dedicated short range communications (DSRC), is a wireless radio technology designed for data transfer in vehicular communications. In 1999 the Federal Communications Commission (FCC) authorized the use of a 75 MHz of spectrum from 5.85 to 5.925 GHz known commercially as 5.9 GHz DSRC band to be utilized for vehicle-to-vehicle (V2V) and vehicle-to-infrastructure (V2I) communications in the United States. Similar DSRC bands exist in Europe (5.855 GHz to 5.925 GHz) and in Japan (5.77 GHz to 5.85 GHz).

The DSRC spectrum in North America is divided into 7 channels with 10 MHz bandwidth for each and 5MHz reserved as a guard band as shown in Figure 1.1. These channels are divided into one control channel (CCH) (channel number 178) and six service channels (SCHs) (Ch 172, Ch 174, Ch 176, Ch 180, Ch 182, Ch 184). There is an option to combine Ch 172, Ch 174 and Ch 180, Ch 182 into two 20 MHz channels namely Ch 175, Ch 181 respectively. High priority short messages or management data are transmitted on the CCH (Ch 178). Two channels (Ch 172, Ch

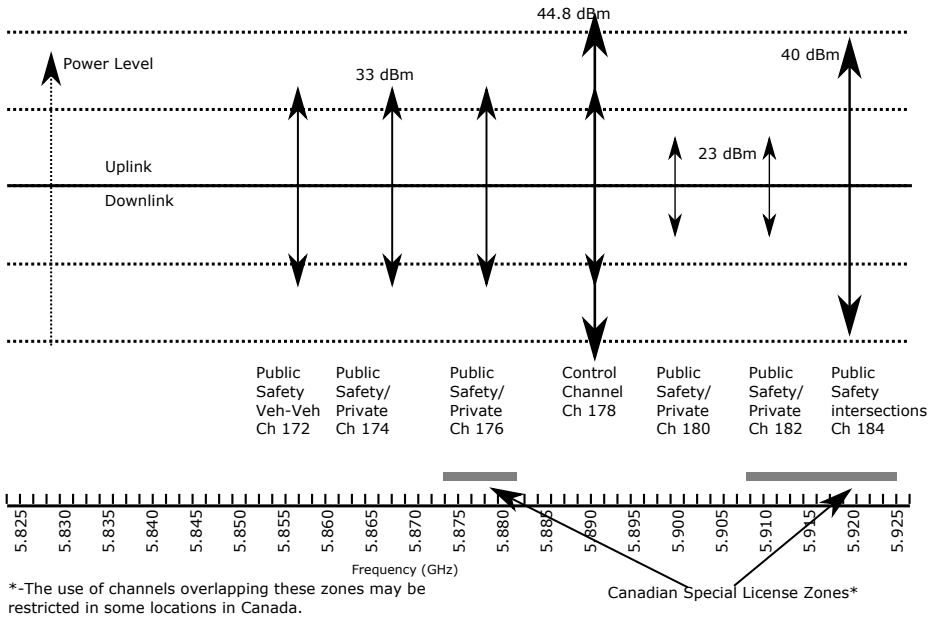

Figure 1.1: DSRC spectrum channels with corresponding allowed channel power [1] [2].

184) are reserved for safety-related applications. The rest of the channels can be used for non-safety communications. Table 1.1 depicts the maximum allowed transmitted power for every channel in North America.

The standard specifications of the DSRC are included in IEEE 802.11p [42] for the physical layer (PHY) and Media Access Control Layer (MAC) layers and the upper layers in the protocol are included in the IEEE 1609 standard [43]. A significant amount of research has been done to define the DSRC link [44] and to also improve the performance of the PHY and MAC layer, namely the packet latency[45].

In [44], narrow band propagation measurements in the 5.9 GHz band to characterize Doppler spread and coherence time in realistic suburban Pittsburgh, Pennsylvania driving conditions. Earlier measurements (1994) [46] centered at the 900 MHz frequency carrier also to characterize the Doppler spread. The Doppler spread was also

Table 1.1: DSRC channel power limitations in North America [1] [2]

Channel Number	Frequency GHz	Maximum Power(dBm)	
		Public Safety	Private Usage
172	5.855 — 5.865	33.0	33.0
174	5.865 — 5.875	33.0	33.0
175	5.865 — 5.885	23.0	23.0
176	5.875 — 5.885	33.0	33.0
178	5.885 — 5.895	44.8	33.0
180	5.895 — 5.905	23.0	23.0
181	5.895 — 5.905	23.0	23.0
182	5.905 — 5.915	23.0	23.0
184	5.915 — 5.925	40.0	33.0

measured at center frequency 2.4 GHz [47]. The vehicular wireless channel models in the literature are valid only for specific vehicular scenario (urban, rural , highway and airport) [48] ,[49]. Where every vehicular scenario is defined by different vehicular traffic density thus Doppler spread values [50].

In [51] the authors measured and modeled a doubly selective channel which is selective in both time and frequency domain, where a selective channel is a channel that degrade the signal components (in time or frequency) with different values. Also in [52] provides analytical expressions for the Doppler spectrum in a mobile radio channel in the presence of multi-path scattering.

More research has been done to examine the usage of the DSRC technology in realistic environments. The simulation model in [53] consists of three vehicles equipped with DSRC units. The results are based on 4 hours drive on highway and 3 hours drive on a test track. The experimental data collected shows 91% packet delivery ratio (PDR) in the highway environment for distances less than 100 m.

The impact of interference on DSRC is quantified in [54] by introducing a jammer to simulate multiple cars interfering with the desired signal to help designing the

setup under heavy channel load. A Different interference mitigation approach is introduced in [55] utilizing a key feature namely "Adjustable Message Frequency". The transmission frequency adapts based on the traffic conditions to avoid overloading the communication channel in the dense traffic scenario. An 80% packet reception rate is noticed at 50 meters with vehicle density of 100 cars per km road.

A simulation setup of a 50 vehicles is presented in [56], with vehicle speed 70 mile/hr, inter-vehicle spacing of 32 meters and driver reaction time is assumed to be 1.5 seconds. The number of vehicles involved in a chain collision is quantified with and without the deployment of a DSRC system with latency 0.1 seconds. The authors claim that they can prevent the collision of the third vehicle in the chain collision using the DSRC system. A 100% of the vehicles will be involved in chain collision if the inter-vehicle spacing is less than 9.6 m at speed of 70 mile/hr regardless of the collision avoidance scheme used.

The DSRC physical layer uses orthogonal frequency division multiplexing (OFDM) which is very similar as the one used in other popular wireless communication channels (e.g. IEEE 802.11a/g standard). Research has shown that the DSRC PHY layer is suitable for low latency safety messages [57]. A few challenges remain, namely when the LOS path is blocked or the channel is experiencing high delay, the communication quality will be degraded and packets might be dropped.

Once a dangerous situation is identified by a CV for example a vehicle running red light, the DSRC MAC layer broadcasts safety message to all CVs in the range of the dangerous situation. This message requires a highly reliable channel with low latency. A probability of reception failure is defined as probability a targeted receiver fails to receive a safety message within a given time delay. The DSRC MAC performance

is quantified using probability of reception failure metric (i.e. message doesn't reach it's destination) in [58], with value of 1/10 for packet repetition higher than 20 times due to the collisions between the broadcasted packets.

The collision probability is decreased in conventional transmission using handshaking signals by having "request to send" and "clear to send" signals before the actual transmission, such a technique is not used with broadcasted messages. Time division multiple access (TDMA) is another way to control the channel access where every vehicle has its own time slot where it listens to the channel or transmit its data. Different MAC layer research has been done relying on the TDMA structure to guarantee the quality of service [59],[45].

1.2 Visible Light Communication

Visible light communication (VLC) is a data communication method using a light source. The idea lies in turning a light source on/off and use it to transmit data. Visible light communication is not a new technology, it has been around for hundreds of years in different forms. It was utilized many years ago in light houses using Morse coded light [60].

Visible light communications is considered to be another form of data transmission using existing infrastructure by modulating light, typically the transmitter is a light emitting diode (LED) and the receiver is a photodiode or image sensors. The use of visible light for communication is motivated by recent developments in LED technology that are leading the way toward their full adoption as a replacement for incandescent and fluorescent lighting [61].

The Visible Light Communications Consortium (VLCC) was started in Japan

in November 2003 to fulfill the aim of developing VLC technologies leading to VLC standards. VLC technology was also evaluated in Europe in the Home Gigabit Access project (OMEGA) started in January 2008, designed to deliver 1 Gigabit/second (Gbps) of internet data by utilizing indoor lighting [62].

The IEEE 802.15.7 standard defines the physical (PHY) and media access control (MAC) layers for optical wireless communications using visible light. The performance of illumination due to modulation is quantified in the standard. The standard supports different data rates from 11 kbps to 96 Mbps for indoor and outdoor applications [63]. The mobility of the visible link, noise and interference from ambient light is also discussed in the standard.

Flicker is a fast change in the brightness of light. The IEEE 802.15.7 standard also complies with the eye safety regulations imposed by IEEE PAR 1789, which regulates the amount flicker LED and avoid any health risks [64]. The IEEE 802.15.7 standard is not the only visible light communication standard available, there are some Japanese standards led by Japan Electronics and Information Technology Industries Association (JEITA) [65],[66].

White light phosphor LEDs are most commonly used in the commercial LED light fixtures [67]. The modulation bandwidth of the white light phosphor LEDs is limited to 2 MHz [68]. In project OMEGA, the bandwidth was increased to 12 MHz [62] by detecting only the blue component of the phosphor LEDs.

For a given bandwidth, bandwidth efficient modulation schemes can be also used to increase the achievable data rate for example pulse amplitude modulation (PAM) or orthogonal frequency division multiplexing, those efficient modulation schemes can be of a great interest in the VLC channel. The signal to noise ratio (SNR) in the

VLC channel is typically in excess of 60 dB electrical which allows the receiver to detect multiple amplitude levels in a signal [69].

Another way to increase the bandwidth efficiency is by generating the white light by using the red-green-blue (RGB) LEDs. Then each color can be modulated separately, such that data is sent on every color wavelength separately in what known as color shift keying [70]. Independent modulation of the colors might create different color than white or changeable light intensity over time [71], [72].

There are various applications that may benefit from the deployment of visible light communication, namely tracking and location based services, for communication where radio frequency is not allowed for example in hospitals and for vehicle to vehicle communication [73].

Location Based Services and Tracking

Bytelight is considered one of the leaders in this area they patented an indoor localization system using LED [74]. The technology relies on the light directionality to provide the user their location and also tracks them if required. The system can provide location specific services or advertisement to the user. The receiver utilizes a rolling shutter camera (defined in section 2.3) to detect the frequency of the transmitted light pulses, where the information is encoded in the frequency of the light pulses.

Radio Frequency (RF) Free Areas

Hospitals and petrochemical production facilities that requires a radio frequency free environment. On going project is happening in Japan that aims to introduce VLC in

the hospitals [75].

Vehicular Communication

Vehicular communication is the main application in this thesis, where vehicles can communicate with each other via either the headlights or the tail lights to warn other vehicles around regarding any sudden stops. A luxury A8 vehicle from Audi was the first vehicle in the market to adopt LED headlamps in 2008 [76].

The emitted light from the LED carries the vehicle information in a wireless medium. The light intensity of the transmitter restricts the transmission range. Literature explored different receiver approaches in the VLC system, namely photodiode receiver, high-speed camera and mobile-phone cameras. In [77] the authors analyze the optical channel behavior in real world vehicular environment settings utilizing off-the-shelf scooter tail light as a transmitter and photodiode as receiver. A complete scooter prototype was developed in [78] to quantize the packet reception rate at different locations during a scooter overtaking scenario. The first packet received by the overtaken scooter happens when the overtaking scooter is 3 meters ahead and more than one second before it intercept the overtaken scooter path.

Performance evaluation of VLC link in an outdoor vehicular environment is examined in [79] utilizing a proprietary test platform the authors show that the VLC link is resilient to sunlight noise under normal operating conditions (less than 100 meters).

Utilizing existing LED lighting in the vehicle tail light or head light, researchers in [80] presented an automobile positioning scheme. The presented scheme provides the driver with vehicle position relative to the surroundings with no cooperation between

different vehicles other than the source transmitting the positioning waveform and the receiver receives the waveform using a photo-detector.

A hardware implementation of infrastructure-to-vehicle visible light communication system for road safety is presented in [81] utilizing LED array as a transmitter and photodetector as a receiver. The authors quantify the system bit error rate and the packet error rate. In this research the authors claims an SNR value of 8 to 10 dB to achieve reliable data reception.

The background noise performance as a function of the time of the day is quantified to be 20 dB between the early morning and peak afternoon in [82]. Utilizing a two lens receiver with a selective combining approach to combine the signals received from the two lens, the coverage range and the received information were found to be limited by the noise value through different times during the day.

A receiver structure was proposed in [83] with a wide-angle camera, narrow-angle camera and photodiode. The bit error rate of the same receiver was quantified in [84] to be 10^{-7} at a date-rate of 2 Mbps in a daytime outdoor environment over 40 meters.

The effect of multi-path delay for VLC channels in a vehicular environment at vehicle speed of $1-5$ km/h is quantified in [85]. The number of multi-path components is assumed to be 6 with 20 nsec delay, and the BER is quantified in a simulation environment.

The VLC link budget analysis is quantified both analytically and experimentally in [86]. The link budget and bit error rate (BER) were evaluated on a transmitter-receiver horizontal separation distance of 5 to 80 meters where the receiver is a photodetector. BER value is approximated to be 10^{-10} at transmitter-receiver separation

distance of 28 meters at a data rate of 4 Mbps assuming dominated input current noise level of 2 $pA/\sqrt{Hz}$.

A hybrid visible light and radio frequency communication system was introduced in [87]. The utilized RF technology is Code Division Multiple Access (CDMA). The VLC signal is used to transmit a location based CDMA code to be used to demodulate the RF signal when the VLC signal is not available.

A bit error rate of 10^{-9} was achieved over a communication distance of 20 meters in daytime outdoor environment using vehicle existing Controller Area Network (CAN) as a transmitter and photo detector as a receiver [88].

1.3 Camera Communications (CamComm)

National Highway Traffic Safety Administration (NHTSA) issued a final rule requiring rear visibility technology in all new light vehicles (under $10,000$ pounds) by May 2018 [89]. The vehicle cameras help the driver detecting objects that do not appear in the rear view mirror for example children. More camera usage is possible, aided by software pattern recognition detecting the speed limit signs and warn the driver whenever the speed limit change, detecting driver fatigue warning with closed eyes or dropped head. Dash cameras to record evidence in case of vehicle crashes as well as for driver leisure taking selfie pictures as in Mini Copper vehicles by integrating GoPro cameras [90]. Also Ford vehicles (S-Max and Galaxy) have a front facing split camera that enables the driver to see objects on blind junctions [91].

Camera Communications (CamCom), is defined as the usage of the cameras for communications, where the camera image sensor is used for data reception. Camera communications utilizes a commonly used visible light sensor which is the mobile

phone camera. The transmitter in a camera communication system could be an LED or an LED display which is modulated to transmit information.

There are two types of camera image scanning, A global shutter camera is a camera that captures the scene details all at the same time. A rolling shutter camera is an imaging receiver which time sequentially expose each row of pixels per frame. The cameras architecture are described in more detail in Section 2.3.

Line of sight marketing is a method to advertise products in the proximity of the targeted audience. The distance range of the targeted users varies depending on the line of sight marketing technology used. For example "QR Code" is one form of line of sight marketing were the targeted users are few cm's away from the QR code pattern. The range of the targeted users by the line of sight marketing can be extended using CamCom [92]. The data transmitted on a CamCom system similar to the same data embedded in QR Code pattern, for example product website and product sale locations. To control the LEDs the system should allow dimming, which can be performed using pulse width modulation [63].

CamCom is also utilized for vehicular communications, the success rate of locating the transmitter is found to be 96% in [93] utilizing a high speed camera as a receiver. The receiver finding algorithm [93] relies on differences between the current frame and pervious frames to locate the transmitter in the image.

1.3.1 Multiple Input Multiple Output Camera Communications (MIMO CamCom)

Multiple research groups carried out research work for vehicle communications using visible light communication technology. Different approaches were evaluated, some

researchers adopted the single element photo detector receiver approach[94]. In [95] the authors observed a packet error rate of 10^{-5} in outdoor bright sunlight environment at transmitter-receiver distance of 10 meters with a data rate link of 20 kbps.

A different receiver approach using high speed camera is evaluated in [96]. In [97], a bit error rate of 10^{-4} is observed at 35 meters away from the transmitter, using a 1000 fps camera and 16×16 LED transmitter array.

In [98], the authors discussed the concept of the optical MIMO using imaging and non-imaging receivers, receiver alignment issues are discussed and evaluated assuming an alignment free receiver architecture. The imaging receiver hardware limitation specifically readout time is not quantified, which could be is a limiting factor especially to achieve the claimed high data rate 48 Mbps for 2×2 LED array (60×60) per array.

A camera image sensor receiver with a hypothetical sampling rate 1 MHz which does not exist in the market yet and multiple array of LEDs as a transmitter are used to achieve visual MIMO communication [99]. In the same study an experimental video was captured at frame rate of 60 fps and the vehicle driving with 25 km/h.

A rolling shutter camera was utilized in [100] to subsample the image, where the transmission frequency of the source is 120 Hz for logic zero and 105 Hz for logic one so that every bit duration is 1/15 seconds i.e. every bit is represented by two samples using iPhone 4 camera at 30 fps. A modulation method namely undersampled Frequency shift ON-OFF Keying (UFSOOK) modulation is defined in [101].

A data rate of 10 Mbps is claimed in [102], [103] utilizing special CMOS image sensor with hardware accelerators fabricated specifically for optical communication as a receiver and 10×10 LED achieving average packet arrival rate of 91% over 5

second transmission in an experimental vehicle with a maximum speed of 25 km/h, where a successful packet is being received when the receiver is able to detect the preamble and the postamble (end of transmission).

1.4 Thesis Organization and Contributions

The remaining parts of this thesis are organized as follows. Chapter 2 presents the essential background necessary to understand the thesis. In Chapter 3, the DSRC radio frequency channel is explained and modeled. The bit error rate performance of DSRC is quantified based on experimental fading channel measurements which are measured and modeled in [9] and is integrated into a vehicle network traffic simulator (will be described in Section 3) [104] to evaluate the safety of the traffic network in terms of collision warning reduction. Similarly in Chapter 4, the visible light communication channel link is modeled and then integrated into the same traffic model to evaluate the safety of the traffic network in terms of collision warnings.

MIMO camera communication is another way to overcome slow data rate problem. Since the transmitter may consist of multiple LEDs, independently modulating each LED with different data stream which creates a multiple input multiple output system (MIMO) adding system performance gains which can be utilized to either improve the system error rate or increase the data rate.

Chapter 5 demonstrates a new approach to MIMO camera communication where data is transmitted by independently modulated multiple LEDs and is received by two inexpensive rolling shutter cameras. The cameras are orthogonal on each other to guarantee independent data samples. Finally Chapter 6 concludes the thesis and future work to be investigated.

The thesis contributions lies in modeling the dedicated short range communications channel to evaluate the link quality performance and joint collaboration between myself and my colleague Mr Genders (McMaster Civil Engineering department) in integrating that channel model into vehicle traffic simulator. With my colleague Mr Genders contribution to this work in producing a statistical results and analysis to quantify the effect of DSRC channel model on vehicular traffic network.

Furthermore, the visible light communication channel is also modeled for vehicular environment and added into the same vehicle traffic simulator. Again with my contribution is developing the communication channel model and my colleague Mr Genders in producing the statistical results and analysis for different market penetration ratio.

Finally, a new methodology to increase the maximum achievable data rate using rolling shutter camera as a receiver and multiple LEDs as transmitter is proposed. An increase of at most double in the achievable data rate using two orthogonal rolling shutter cameras as receivers and $2^i \times 2^i$ LEDs organized in a square matrix compared with the usage of the same transmitter and only one rolling shutter camera as a receiver. This data rate increase is achievable only utilizing a novel receiver architecture which enables a new paradigm shift in the camera communications systems compared with the previous literature.

Chapter 2

Background

In this chapter the fundamentals necessary to understand the work done in this thesis are presented. The chapter discusses the basic knowledge of radio frequency communication, channel effects on RF wireless signals and various methods to overcome such effects. Then the basics of visible light measurement units that quantifies light nature. Finally camera imaging technologies and fundamentals are presented.

2.1 Radio Frequency

Radio frequency (RF) is an electromagnetic wave that propagates through a medium and have frequency that ranges from 3 Hz to 300 GHz. Market development in the recent years demanded devices wireless connection for a broad range of products starting from phone calls to remotely controlled houses [105], that lead to a congested interfered air medium. The remaining part of this section will address radio frequency multiple access. Then the RF channel characteristics is discussed. Finally an example of channel coding namely Reed Solomon coding is presented.

2.1.1 Radio Frequency Channel Characteristics

The characteristics of the wireless signal when it travels from the transmitter antenna to the receiver antenna need to be carefully modeled. The received signal strength depends on the distance between the transmitter and the receiver and the path the signal traveled in for example was it line-of-sight path / non-line-of-sight path or fixed/mobile link.

The received signal is defined as $y(t)$

$$y(t) = h(t, \tau) * x(t) + n(t) \tag{2.1}$$

where $x(t)$ is the transmitted signal, $h(t, \tau)$ is the random channel impulse response and $n(t)$ is the noise.

The received signal undergoes different effects namely the path-loss, shadowing and multi-path. *Path-Loss* is the loss in the transmitter signal power where the transmitted signal energy attenuates as it spread in a spherical way. This loss is proportional to the transmitter-receiver distance. Friss equation is a simple mathematical way to represent the relation between the wireless received signal power and the transmitted signal power. The equation was derived in 1945 by Harald Friss [106].

Shadowing also affects the transmitted radio signal. It occurs when the propagation path between the transmitter and receiver is obstructed causing signal power loss. Shadowing arises due to various reasons namely when the transmitted signal is scattered or diffracted causing signal power loss. Also when the transmitted signal is reflected, portion of the signal power is absorbed on the reflection surface causing signal power loss. Figure 2.1 depicts an illustration of a transmitted radio signal from the transmitter to the receiver that faces shadowing due to diffraction and reflection

from building surfaces.

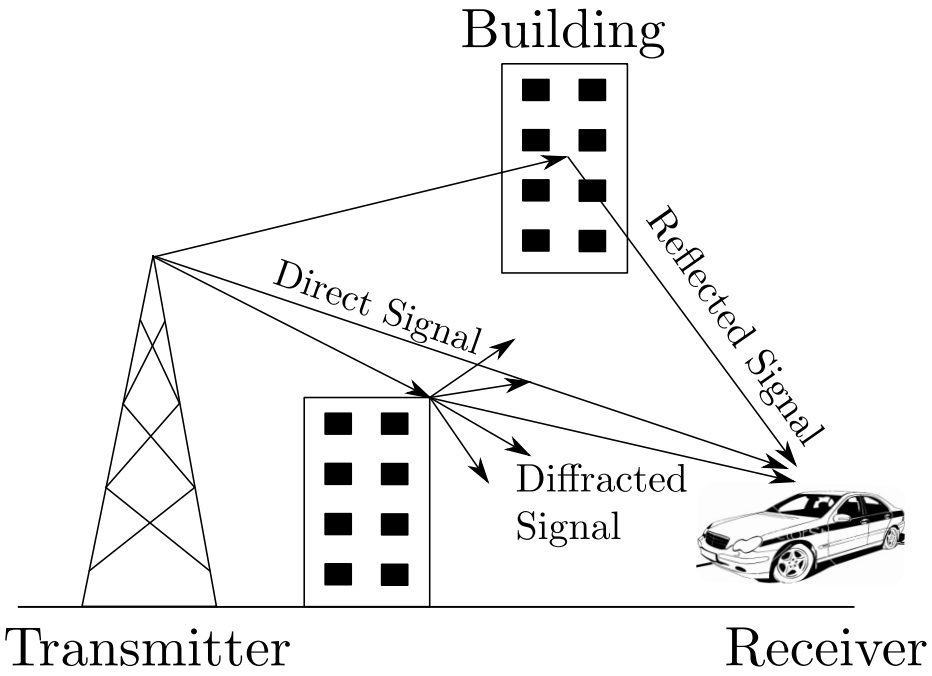

Figure 2.1: An illustration for a transmitted radio frequency wave, the transmitted signal experience shadowing due to diffraction and refection from building surfaces.

Figure 2.2 depicts the multi-path signal phenomena, each reflected signal takes random path which results in different amplitude and phase for the received replicas. Depending on the received signal phase and magnitude the received replicas can add together constructively or destructively.

Coherence bandwidth is defined as the bandwidth over which the channel frequency response is considered constant. The multi-path causes a signal fading, this fading is characterized into flat and frequency selective fading. A flat fading occurs when the signal bandwidth is less than the coherence bandwidth of the channel and frequency selective fading occurs when the signal bandwidth is more than the coherence bandwidth [107].

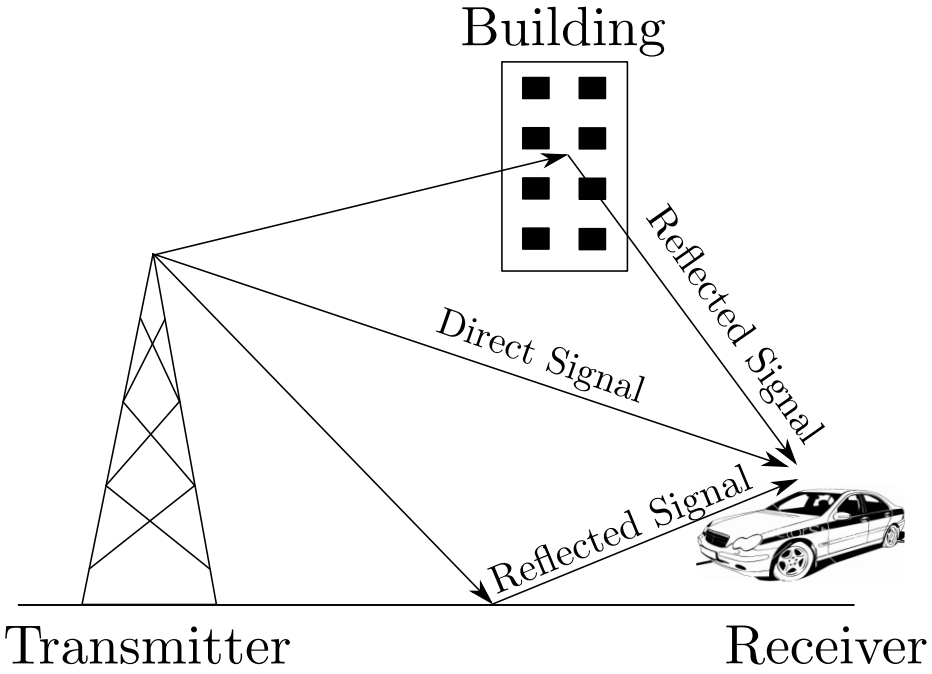

Figure 2.2: An illustration for a radio frequency transmitted signal multi-path, different signal replicas arriving at the receiver from different paths.

The channel effects described previously affects the transmitted signal causing signal losses. The channel impulse response defined in equation 2.1 is given by

$$h(t,\tau) = \sum_{i=1}^{N} L_i(t,\tau) z_i(t,\tau) \delta(t-\tau_i) \tag{2.2}$$

where N is the number of multi-path components, $L_i(t,\tau)$ is the path-loss for the ith multi-path component, $z_i(t,\tau)$ is random variable drawn from a fading random distribution and τ_i is the ith multi-path excess delay.

One way to overcome this signal loss is channel coding. In the next section, Reed Solomon Coding is introduced.

2.1.2 Reed Solomon Coding

In order to overcome the channel limitations presented in Section 2.1, added redundancy on the transmitted data is needed to be able to recover the original transmitted message, one way to add such redundancy is channel coding. The channel code used in this thesis is Reed Solomon code.

In this thesis Reed Solomon code is used as a digital fountain code [108]. Despite existence of other digital fountain codes for example Raptor codes [109], LT codes [110], Reed Solomon is used due to its widespread use.

Data recovery or in other words, error correcting codes has various classifications namely block codes and convolutional codes. Reed Solomon code is a block code. The transmitted message is divided into a sequence of data blocks before getting transmitted on the channel medium. Each data block then have parity information appended to it to create a code word. Reed Solomon code is generally used as a systematic code such that the data is transmitted as is and then appending the

parity check bits at the end of the block.

One of the important features in the Reed Solomon code is that it is a linear code such that if two code words are added together the results is also a code word, another feature is that cycling shifting of one code word also produces another code word, in other words, they are linear cyclic codes.

The code error correction ability is determined based on the code parameters, affecting the implementation complexity as well. A Reed Solomon code is characterized by two parameters n, k where k is the number of the information symbols in the codeword and n is the block length in symbols with an upper bound $2^m - 1$ where m is the number of bits in one symbol.

The code is able to correct t symbol errors and $2t$ symbol erasures. where $t = (n-k)/2$ for $n-k$ even and $t = (n-k-1)/2$ for $n-k$ odd.

The syndrome values indicate an occurrence of an error as they are not zero values. Serval decoding algorithms utilizes the syndrome values to detect the location of the error and correct it namely *Euclid's Algorithm* [111], *Berlekamp-Massey Algorithm* [112] and *Peterson-Gorenstein-Zierler Algorithm* [113].

2.2 Visible Light Characteristics

Visible light is a form of electromagnetic energy traveling in the space. Visible light has a wavelength (λ) of 400 to 700 nm. Incoherent light sources electromagnetic waves interfere with each other and get directionally polarized and bend when it passes an edge. In radiometric properties, the light is considered as a ray traveling in a straight line where optical components such as lenses and mirrors can redirect those rays in different predefined paths. The rest of this section will describe in detail the visible

light measurement units as well as the visible light wave properties.

2.2.1 Radiometric and Photometric

The fundamental unit of power measurement is the *watt*, defined as the rate of energy (joule) per second. The optical power is function of number of photons and the energy of every photon as well as the rate of photon arrival. Photon energy is quantified as $Q = hc/\lambda$ joules where h is planck constant $= 6.623 \times 10^{-34}$ and c is the speed of light $\approx 3 \times 10^{8}$ and λ is the light wave length.

Measuring the light as it is perceived by the human eye is defined as photometry. In photometry the equivalent of the Watt is the Lumen (lm), which is defined as the weighted power to match the eye response of a standard observer. The human eye normalized sensitivity to different light wavelength is $L(\lambda)$ [114]. The Lumen is given by

$$\Phi_L = K_w \int_{\lambda=380}^{\lambda=780} P(\lambda)L(\lambda)d\lambda \tag{2.3}$$

where $P(\lambda)$ is the light source spectral power density and K_w is the maximum luminous efficacy (lumen/watt).

The human eye can see flux of approximately 10 photons per second at a wave length of 555 nm, which is equivalent to radiant power of 3.58×10^{-18} watts. Similarly the eye can see minimum flux of 214 and 126 photons per second at 450 and 650 nm respectively [3].

Steradian is considered one of the key concepts to understand the relationship between different measurements. Figure 2.3 shows the definition of the steradian angle, it is defined as the solid angle which have its vertex at the center of the sphere and it cuts the sphere in a surface area equal to the square of the radius of the

Figure 2.3: Left figure shows a steradian angle ϕ removed from the whole sphere. On the right steradian angle ϕ is calculated .

sphere, a sphere contains 4π steradians. The solid angle of the cone ϕ in steradians is $\phi = A/r^2$, where A is the area of the portion of a spherical surface subtended by the cone and r is the sphere radius .

However in most of the radiometric measurements, an accurate representation of the spherical area is not necessary to convert between units, and the flat area can be used as an approximation for the spherical area for small solid angle $\leqslant 0.03$ which gives an error of 1% [3].

Radiometric power is measured in radiant flux which is defined as the rate of energy (in joules) per second which is Watts. Photopic flux is defined as lumens which is filtered to match the eye response. Luminous flux, 1 lm (lumen) = 1.464×10^{-3} Watts at 555 nm.

Irradiance is the measurement of the flux density defined in Watts/m^2 and illuminance is the measure of flux per unit spherical surface area (Figure 2.3), visible flux density in lux.

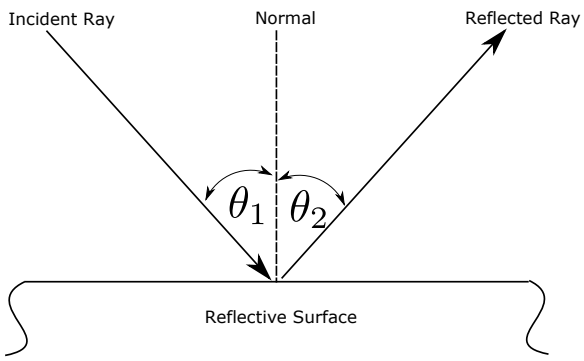

Figure 2.4: Law of Reflection [3].

2.2.2 Light Properties

Reflection

Figure 2.4 depicts an incident light hitting a reflecting surface. The light rays reflect back following the law of reflection. The incident angle (angle between the normal to the surface and the incident ray) is equal to the reflected angle (angle between the reflected light and the normal to the surface) Figure 2.4. Another form of light reflection namely diffuse reflection occurs when incident light hits a rough surface, the reflected light rays reflect in all angles.

Refraction

Snell's Law explains refraction, when a light passes two different mediums with different refractive indexes, light rays experience a change in their velocity and their direction bends. The factor that governs this phenomena is the incident angle and the refractive indexes of the two mediums.

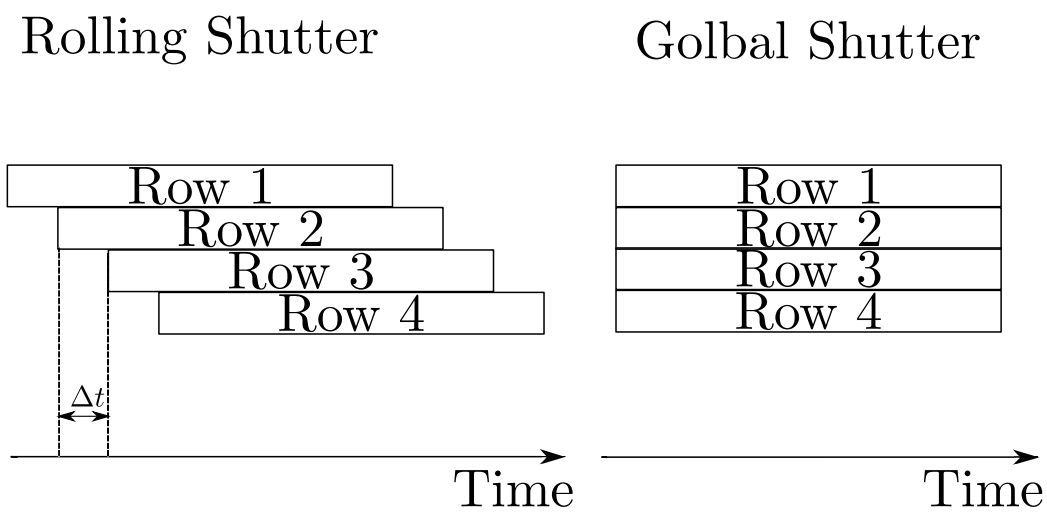

Figure 2.5: Left: Diagram demonstrating rolling shutter time delay (Δt) between each row of pixels in an image. Right: Diagram showing no delay between row of pixel in an image utilizing global shutter camera.

2.3 Rolling Shutter and Global Shutter Cameras

There are two different ways for image scanning. The first one where the camera take an image of the whole scene all at once as if its frozen, known as global shutter. The whole frame is read once all together. It is known to be the most accurate representation of the motion especially in the fast motion events because the captured image is a frozen scene captured at specific time instant [115].

However, to increase the frame rate, each row in the image is exposed to the light independently as an image scanning mechanism known as *rolling shutter*. Figure 2.5 depicts the rolling shutter image scanning algorithm such that each line in the image is scanned at different time with offset (Δt) of the readout time for each line [116].

2.3.1 Stereo Vision

Stereo Vision, is the science of recovering of a $3D$ image data using two $2D$ images of the same scene captured from two different points, those two images could be obtained from multiple cameras or from one moving camera.

The $3D$ recovery is done using triangulation principle, where the location of the point in $3D$ is determined by the projection of the point in the camera's image plane, provided that the relative position between the cameras is defined.

Figure 2.6 depicts an example of sample object (e.g., a maple leaf) and two cameras are capturing the image of the scene. The cameras are placed with distance b apart from each other. The resultant images for camera 1 and camera 2 are shifted in the horizontal axis with respect to each other [117]. The object is located at x_1 and x_2 in the captured images respectively. From the ray theorem of geometry [118] the shift in the resultant captured images in the horizontal axis ($x_1 - x_2$) is quantified as follows

$$x_1 - x_2 = \frac{f \times b}{d} \tag{2.4}$$

where f is the cameras focal length, b is the cameras horizontal separation distance and d is the object distance from the cameras image plane. In this setup the cameras are aligned such that their optical axes are parallel thus results in image on the second camera is shifted to the right (i.e. $x_1 > x_2$).

2.4 Conclusions

This chapter presents the fundamentals required to understand the thesis. In this chapter the fundamentals of radio frequency are presented, different methods of radio

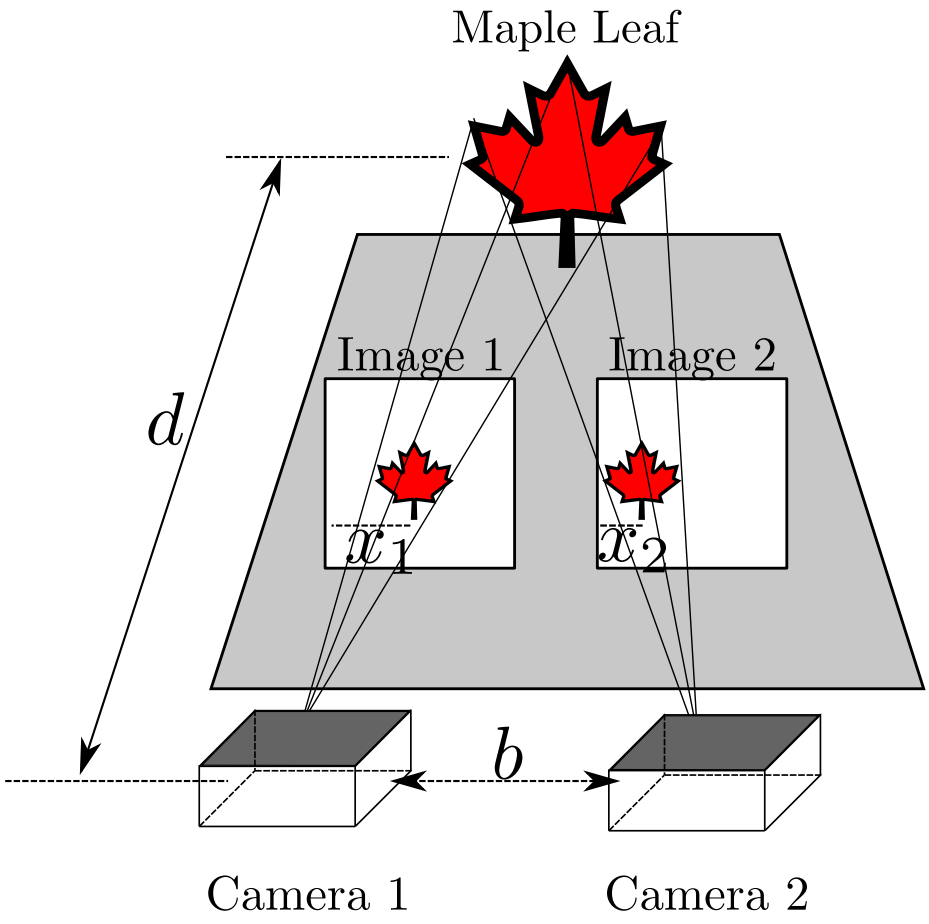

Figure 2.6: An illustration of stereo vision concept using a maple leaf object located at distance d away from two cameras, the two cameras are located on the same horizontal plane with a separation distance b.

frequency multiple access are introduced. The radio frequency channel characteristics namely shadowing, path-loss and multi-path are described. Furthermore an example of channel coding (Reed Solomon coding) to overcome the wireless channel effects is also introduced.

The visible light have a unique characteristics that combine between wave and particle properties. The measurement units that quantify both the wave and particle properties of the light are introduced in this chapter as well as the conversion between those units.

The chapter concludes with introducing different camera imaging scanning algorithms namely rolling shutter and global shutter. The timing diagrams in the rolling shutter and global shutter case are discussed. Finally, the stereo vision concept in cameras is introduced.

Chapter 3

Dedicated Short Range Communications

This chapter quantifies the impact of communication degradation in a vehicle-to-vehicle (V2V), forward collision warning (FCW) application (see Figure 3.1). A dedicated short range communication (DSRC) channel model is used where path-loss, penetration-loss and interference are quantified. A section of Toronto, Ontario, Canada is modeled in a traffic micro-simulator to evaluate the effects of the channel model on V2V communication. Various market penetrations of Connected Vehicles are simulated using two communication models; the first an ideal channel and the second a DSRC channel which quantifies the impact of channel impairments. The purpose of the forward collision warning application is to warn the driver of an imminent collision with the leading vehicle. The surrogate safety measure of improved Time to Collision is used as a metric to evaluate the effectiveness of the forward collision warning.

A collaborative effort between myself and Wade Genders was utilized to produce

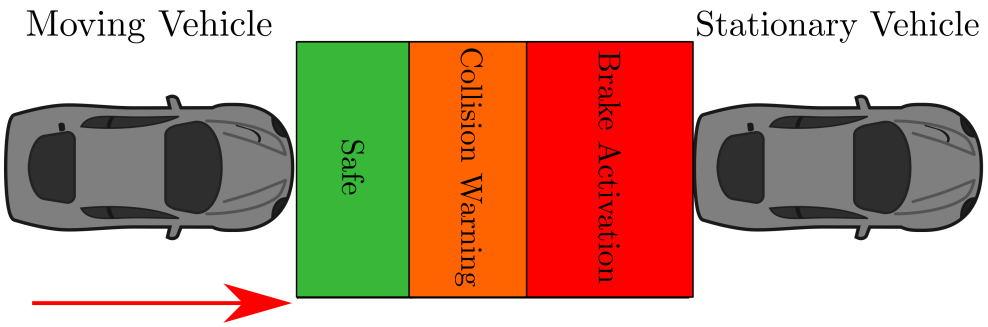

Figure 3.1: Forward Collision Warning application

the results in this chapter and chapter 4. In this chapter my contribution is the wireless communication channel model and Wade Genders contribution is the vehicular traffic simulator, similarly in chapter 4. Where my contributions lies in section 3.1.1 and section 3.2 and my colleague Wade Genders contributions are in section 3.1.2 and section 3.2 .

Connected Vehicles seek to improve current transportation methods through the integration of computing technologies, which aims to improve the safety, mobility and environmental impacts of transportation via real-time data sharing between vehicles and infrastructure. In this chapter Connected Vehicles are considered with dedicated short-range communications (DSRC) to facilitate wireless communications from vehicle-to-vehicle (V2V) and vehicle-to-infrastructure (V2I).

Although many improvements have been made in an effort to improve vehicle safety, accidents and fatalities still occur. Rear-end collisions are one of the most common forms of accidents [119]. Connected Vehicle can offer forward collision warning (FCW) via V2V communication to prevent these incidents from occurring.

The remainder of this chapter is organized as follows. Section 3.1.1 presents the DSRC channel model and section 3.1.2 presents the traffic simulator. Performance

results are presented in section 3.2 and the chapter concludes in section 3.3.

3.1 System Model

3.1.1 Dedicated Short Range Communications Model

Dedicated short range communications are primarily allocated for vehicle safety applications, particularly in Connected Vehicles. Despite the desirable features of the DSRC for safety applications its use in dense urban environments face important limitation caused by interference as the received DSRC radio signals are corrupted by reflections, scattering and absorption by the objects located in the transmission path.

The channel effects namely path-loss and multi-path fading can be divided into two categories: large scale fading and small scale fading. Path-loss inherent to radio propagation is a fundamental form of large scale fading. Penetration-loss is another form of large scale fading which occurs when there is a large obstacle, such as another vehicle or building, in the propagation path causing major absorptive losses, a more detailed description of channel effects is presented in section 2.1.

Table 3.1 lists typical values for the physical layer parameters of a DSRC system using orthogonal frequency-division multiplexing (OFDM), where information is transmitted on multiple orthogonal frequency channels to overcome channel fading [1].

The large scale path loss factor, L_{FS}, in an urban environment can be modeled as [120]

Table 3.1: DSRC OFDM Parameters [1]

Parameter	Value
Frequency Band	5.9GHz
Channel Bandwidth	10 MHz
Supported Data Rate	$3, 4.5, 6, 9, 12, 18, 24$ and 27
Modulation	BPSK, QPSK, 16QAM and 64QAM
Channel Coding	Convolutional Coding, Rate $1/2, 2/3, 3/4$
Data Subcarriers	48
Pilot Subcarriers	4
FFT size	64
FFT Interval	6.4μS
Subcarrier Spacing	156.25KHz
CP Interval	1.6μS
OFDM Symbol Interval	8μS

$$L_{FS} = \begin{cases} 20\log\dfrac{\lambda}{4\pi d}, & d \leqslant d_0 \\ 20\log\dfrac{\lambda}{4\pi d_0} - 10n_0\log\dfrac{d}{d_0}, & d_0 \leqslant d \leqslant d_1 \\ 20\log\dfrac{\lambda}{4\pi d_0} - 10n_0\log\dfrac{d_1}{d_0} - 10n_1\log\dfrac{d}{d_1}, & d > d_1 \end{cases} \tag{3.1}$$

where λ is the wavelength, d_0, d_1, n_0, n_1 are path-loss parameters defined as $d_0 = 15$ m, $d_1 = 1000$ m and $n_0 = n_1 = 4$ in non line of sight dense urban environment [120].

In an urban environment, typical outer wall penetration loss for high rise buildings is $L_{ow} = 1.93$ dB and the inner wall penetration is $L_{iw} = 1.75$ dB [121] . In this work, all buildings are modeled under the assumption of having an inner wall every 4 meters.

Small scale fading consists of multi-path fading which arises from the reception of multiple copies of the transmitted signal due to reflections in the environment [107]. These delayed and attenuated receptions (channel taps) result in a random time-varying fading loss in the channel.

The multi-path fading is modeled following the study of Sen and Matolak [9] which

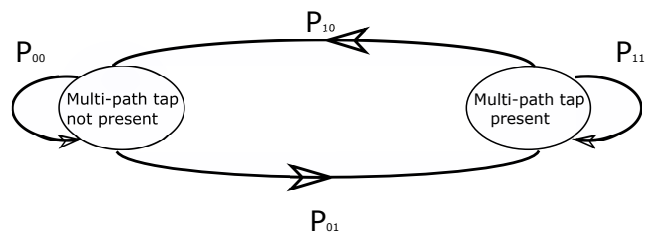

Figure 3.2: State transition diagram for two state Markov process modeling appearance of multi-path taps.

used curve fitting of numerical measurements to create probabilistic models. In [9], the number of multi-path channel taps are determined by the maximum root mean square delay spread (RMS-DS) and then the average energies of each multi-path tap are found by averaging over power delay profiles (PDPs). Only those tap samples for which relative energy is above the threshold (25 dB below the main tap) are considered. The probability density function (PDF) of the nth tap random variable z_n is modeled by a Weibull probabilistic fading model

$$f(z_n; \Lambda, k) = \frac{k}{\Lambda^k} z_n^{k-1} \exp\left[-\left(\frac{z_n}{\Lambda}\right)^k\right] \tag{3.2}$$

where k is a shape factor that determines fading severity, $\Lambda = \sqrt{E(z_n^2)/\Gamma[(2/k)+1]}$ is a scale parameter and Γ is the gamma function. This fading distribution is utilized in the channel effect as random variable drawn from the probabilistic distribution as discussed earlier in equation 2.2.

Figure 3.2 depicts an on/off two state Markov chain, where the reception of a signal from a certain multi-path (channel tap) at a certain time is modeled as Markov chain with transition probability parameters stated in Table 3.2.

Table 3.2: Channel Models for 10MHz Channels in Urban outdoor Antenna [9, Tbl.V]

Tap Index (n)	Energy (E_n)	Weibull k	P_{00}	P_{11}	P_1
0	0.88	3.19	NA	1	1
1	0.08	1.61	0.2717	0.9150	0.8956
2	0.03	1.63	0.4401	0.8171	0.7538
3	0.01	1.73	0.5571	0.7488	0.6382

The channel is given by

$$h(\tau_n, t) = \sum_{n=0}^{n=3} E_n \times P_1 \times z_n \times L_{FS_n} \times L_{ow_n} L_{iw_n} \times \delta(t - \tau_n) \tag{3.3}$$

where, n is the multi-path tap index, E_n is the tap energy as defined in table 3.2, P_1 is the tap steady-state probability defined in table 3.2 . L_{FS_n}, L_{ow_n} and L_{iw_n} are the path loss for tap number n, outer wall penetration loss and inner wall penetration loss respectively. The multi-path tap delay τ_n CDF is quantified in [9, Fig. 2] by utilizing channel measurements for 6000 power delay profiles. The root-mean-square delay spread mean is 125.8 nsec [9, Tbl. II]. In this thesis $\tau_n = n \times 100$ nsec. A random variable z_n is drawn from Weibull probabilistic fading model (equation 3.2) for tap number n with it's corresponding k value.

Interference

Interference from neighboring vehicles is also a major source of degradation in the DSRC channel. In the DSRC channel model used in this work interference sources within 100 meter range from the receiver are considered. Interference is modeled as noise which is independent from the signal of interest and Gaussian distributed. The interference is also dependent on how the six available DSRC OFDM channels are assigned to users in the network. In this work, the DSRC performance is quantified

in two scenarios. In the first scenario, a *random scheduler* assigns channels randomly amongst users that are in range. The second scenario uses a *partitioning scheduler* is an optimistic assignment to ensures that the five strongest interferes are assigned to disjoint channels.

The optimistic DSRC channel performance is integrated into the vehicular traffic simulator to model the communication between every communicating vehicles with an aim to quantify the performance of forward collision warning.

In this chapter, Connected Vehicle V2V communication is modeled at a frequency of 10 Hz [122] to meet latency requirements, exchanging data which is used as input to the FCW algorithm. A leading vehicle transmits a data packet consisting of its current position, direction and speed to all Connected Vehicles within range. The complete DSRC channel model consisting of OFDM modulation, channel realization and detection is implemented to determine if the packet transmission between vehicles is successful. The DSRC channel model in this study is updated at a frequency of 1 Hz. The FCW will attempt to activate at a frequency of 1 Hz. If a following vehicle successfully receives at least 1 of the 10 packets, the FCW algorithm is executed.

3.1.2 Vehicular Traffic Model

In order to quantify the effect of the communication channel model in vehicular environment two different approaches are possible, the first approach is implementing a large scale infrastructure to allow testing of Connected Vehicles in a realistic large scale environment this approach was adopted by University of Michigan by building 32-acre city to allow testing of Connected Vehicles in a realistic, controlled and safe environment [123].

In this thesis we adopt the less expensive second approach which is the computer simulations, in collaboration with McMaster Civil Engineering department, namely Dr. Saiedeh Razavi and Wade Genders. **This section is my colleague Wade Genders contribution to this work**.

The microscopic traffic simulation software Paramics [124] was used to conduct simulations for this research. The microsimulation software simulates each vehicle as an independent entity attempting to create a larger traffic network. The likelihood of a collision is quantified in a safety measure metric. The Time-to-Collision (TTC) (equation 3.4) developed by [125] is used in this thesis as a safety measure metric to quantify the likelihood of a rear-end collision to occur.

$$TTC \triangleq \frac{d_{LF}}{V_F - V_L} \tag{3.4}$$

where d_{LF} is the distance between leading and following vehicle, V_F is the velocity of following vehicle and V_L is the velocity of leading vehicle. A driver reaction time threshold of 1.5 seconds is assumed and a rear-end collision is declared if the TTC is less than the threshold.

A part of Toronto, Ontario Canada was replicated in Paramics for simulation Figure 3.3. A data survey from Transportation Tomorrow Survey [126] was utilized to model the traffic demand for every road. The traffic demand matrices were modeled by representing the number of vehicles entering the vehicular traffic network starting in an origin point and ending in destination. In order to model traffic congestion, the traffic demand matrices were decreased by 35%. The simulation time is 1 hour and 15 minutes, where the first 15 minutes are used to populate the vehicular traffic network.

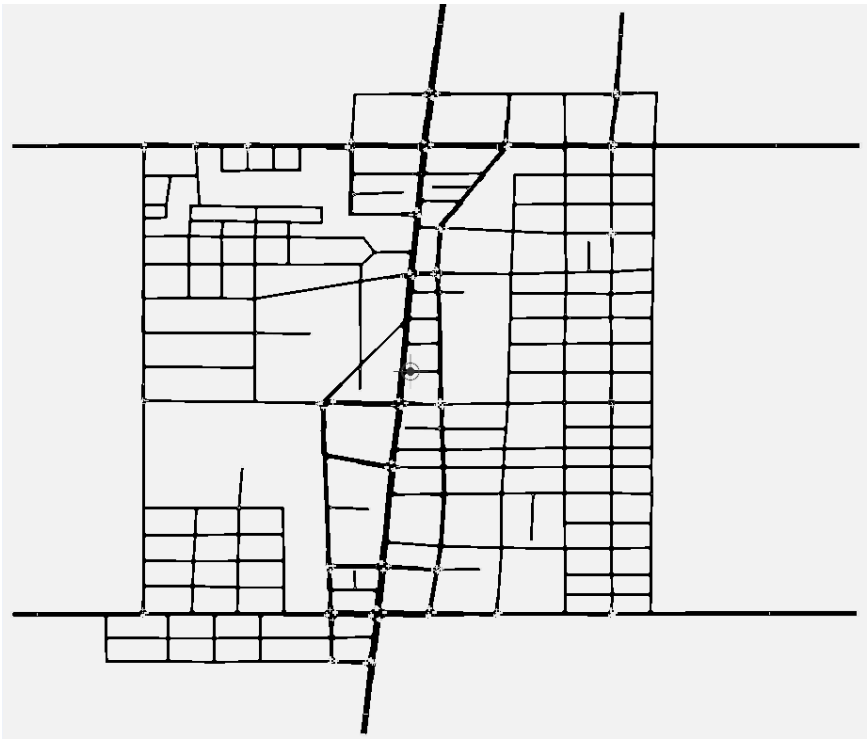

Figure 3.3: Map of the traffic network, Yonge & Shepppard, Toronto, Ontario, Canada, used in this work (near $43^o45'41.4"$N $79^o24'39.1"$W). Simulation area is 2 km$\times$2 km [4].

The forward collision warning algorithm calculates the time collision (TTC) between a following Connected Vehicle (receiver) and a leading Connected Vehicle (transmitter). A FCW is issued to the driver if the computed TTC value is less than 3.0 seconds (FCW threshold). The FCW threshold used in this thesis is more conservative threshold than the one used in the United States National Highway Traffic Safety Administration (4.0 seconds) [127]. In this research it is assumed that the driver will decelerates once FCW is issued.

There are different variables that affects the Connected Vehicle deceleration rate namely the vehicle speed at the instant of issuing the FCW and the distance available to decelerate. Research have shown that decelerate rates range from 0.28 - 4.9 m/s^2 [128][129][130]. In this thesis it is assumed once a Connected Vehicle receives a FCW the Connected Vehicle / driver will decelerate at a rate of 3.0 m/s^2.

3.2 Performance Results

In this section the simulation results for the model discussed in section 3.1 are presented. The performance is evaluated for every transmitter-receiver pair throughout an hour simulation by transmitting 10^5 OFDM symbols per each transmitter-receiver pair, calculating the bit error rate (BER) for every Tx-Rx pair and then calculating the cumulative distribution function (CDF) curves. The BER performance under different Connected Vehicle market penetration ratios namely $10\%, 50\%$, and 100% is quantified and presented in Figure 3.4. At a 10% market penetration using the partitioning scheduler increases the percentage of vehicles achieving BER less than 10^{-3} from 40% to 70%. For 100% market penetration the same percentage increased from 5% to 15%. For the remainder of the chapter, the partitioning scheduler is used

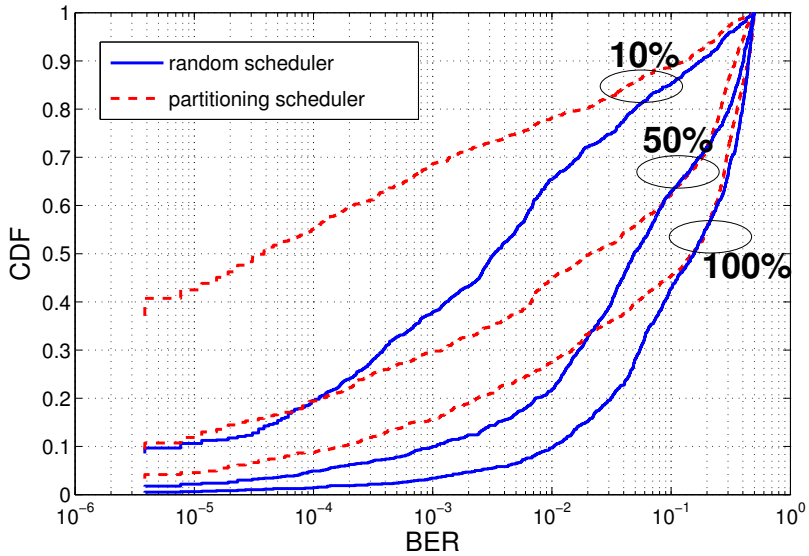

Figure 3.4: DSRC BER CDF performance using random and partitioning schedulers for Connected Vehicle market penetrations of 10, 50 and 100%.

to model the interference present in the DSRC channel model.

To assess the impact of the Connected Vehicle FCW on traffic safety, TTC values are calculated for every vehicle, every second of the simulation. Simulations with a higher number of *critical TTC events* (0 s $< TTC <$ 1.5 s) indicate more instances of potential collisions.

My colleague Wade Genders carried out a vehicular traffic simulations which was tested under 5 different initial conditions, with market penetrations of 0, 5, 20, 40 and 60 % Connected Vehicles using the developed DSRC channel model. The simulation is then rerun without the DSRC channel model and all V2V communications attempted are successful. The results are then partitioned into two categories: ideal and realistic V2V DSRC. Twenty five simulation iterations are completed for each communication category and Connected Vehicle

market penetration. Each simulation iteration is assigned a random seed value, which introduces an element of simulation randomness. Different seed values control simulation aspects such as when vehicles are released into the network, ensuring no two simulations are the same.

Connected Vehicle FCW algorithm execute at a frequency of 1 Hz, but the V2V DSRC attempts to communicate at 10 Hz. For the FCW to be triggered, at least one of the ten V2V DSRC packets must be successfully received at the destination. The total number of FCW issued are the instances where at least one V2V DSRC was successfully transmitted from the leading vehicle to the following vehicle and the calculated TTC was below the FCW threshold.

Considering that as the market penetration of Connected Vehicles increases, a larger proportion of vehicles are transmitting RF signals, i.e. higher interference and packet loss. Packet loss at high market penetration implies that many potential FCWs are not issued because the V2V communication is unsuccessful. If a following vehicle does not receive at least 1 data packet from the leading vehicle, the following vehicle's FCW algorithm cannot execute.

Recall, the safety measure TTC was used as a criteria to evaluate the potential for a rear end collision. Define a *critical TTC event* as the the event that ($0 \text{ s} < TTC < 1.5 \text{ s}$). Additionally, let $NTTC$ denote the number of such events that occur during the simulation time. A larger $NTTC$ implies more instances of a possible collision between following and leading vehicles. As a baseline, define $NTTC_c$ as the number of critical TTC events recorded when the market penetration is 0%. **Wade Genders provided the statistics of the control group determined over 60 simulation**

Table 3.3: Control Simulation Statistics (Wade Genders contribution)

	Critical TTC Observations
Connected Vehicle Market Penetration (%)	(μ,σ)
0	(3529.7, 107.89)

runs in Table 3.3. Define the normalized number of critical TTC events, η as

$$\eta \triangleq \frac{NTTC_x}{NTTC_c} \tag{3.5}$$

where $NTTC_x$ is the mean critical TTC observations at market penetration X%.

My colleague Wade Genders defines η as a metric of FCW effectiveness. At high market penetrations of CVs, η of the DSRC channel model simulations is higher (i.e. more high probability instances of rear-end collisions) compared to the simulations where the ideal model is used (Figure 3.5). This indicates that many instances that would have issued a FCW from a following vehicle did not occur due to unsuccessful communication.

The simulation results provided by Wade Genders showed that when an ideal channel model is used (i.e., all V2V DSRC communications are successful), an 33% reduction in η can be observed at 60% market penetration of Connected Vehicles. At the same market penetration, when considering the DSRC channel model, the η decreases by approximately 22% from the ideal control case.

At market penetrations above 40%, the difference in means accelerates as the market penetration increases. At Connected Vehicle market penetrations of 20% and below, DSRC performance does not degrade. However, above 40%, V2V DSRC suffers.

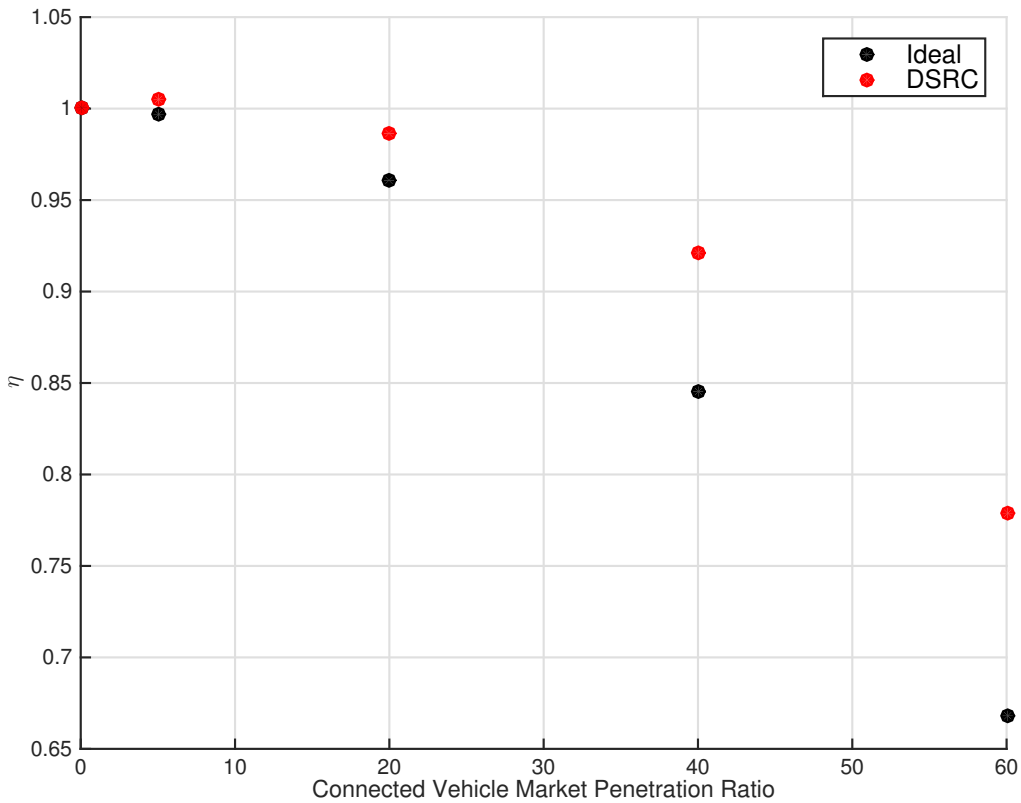

Figure 3.5: Variation of η over Connected Vehicle market penetration. This figure is my colleague Wade Genders contribution based on the DSRC channel model as input to the vehicular traffic simulator.

3.3 Conclusion

Connected Vehicles have the potential to improve transportation safety, mobility and sustainability through information sharing. Wireless communication via V2V DSRC can potentially benefit many Connected Vehicle applications, but understanding its limitations is important to optimizing its use.

Many *critical TTC* situations involving a leading and following vehicle did not receive a FCW due to lost V2V DSRC packets. The potential improvements in mitigating rear-end collisions are large, as when simulating a perfect channel, an 33% reduction in rear-end collisions was observed. Visible light communications (VLC) is a potential candidate communication technology which can succeed when DSRC performance degrades, retaining successful communication probability at high market penetrations. VLC will be studied in tandem with DSRC in the next chapter.

Chapter 4

Visible Light Communication

4.1 Introduction

This chapter illustrates the visible light communication channel model. In the vehicle to vehicle communication model the vehicle ahead receives light from the LOS component of the vehicle behind as well as the reflections from the road. The vehicle low beam headlamp radiation beam pattern is modeled, line-of-sight component and the reflections from the ground. Different weather conditions clear, rain, fog and snow are also considered. **Similarly as in Chapter 3, this chapter is a collaborative work between myself and Wade Genders where my contribution is the visible light communication model and Wade contribution is the vehicular traffic model statistics**. The visible light communication model is utilized in the Toronto downtown vehicle network simulator to quantify the safety in the vehicular network.

4.2 Visible Light Communications Channel Model

Visible light communications combines illumination and communication functions using commercially available visible light LEDs [131]. In this study, V2V VLC model in [6] is considered and combined with the DSRC model of Chapter 3 to assess the impact of different individual or hybrid communication methods on the V2V-based forward collision warning.

This section illustrates the visible light communication channel model. The basic scenario for the V2V communications occurs where the following vehicle receives light from the line-of-sight (LOS) component of the vehicle ahead as well as the reflections from the road surface, Figure 3.1 depicts the forward collision warning scenario. The vehicle tail-light radiation beam pattern is modeled including line-of-sight component and the reflections from the ground. Different weather conditions including clear sky and low visibility weather are also modeled.

The VLC transmitter will typically consist of an LED illuminator in the tail-light of a vehicle. A market-weighted report measures the the luminous intensity (cd) $I(\alpha, \beta)$ for different vehicles manufacturers and then averages those patterns according to the top 90% USA vehicles sales is presented in [5]. In this work a scaled down market-weighted low-beam headlamp pattern [5] is used to model the emission pattern of the tail-light. The emitted optical power is scaled by a half to correspond to a tail-light emission [132].

Figure 4.1 depicts the 50% percentile of the low-beam headlight beam pattern with a lamp mounting height: 0.66 m and a lamp separation 1.20 m [5].

The received power is given by:

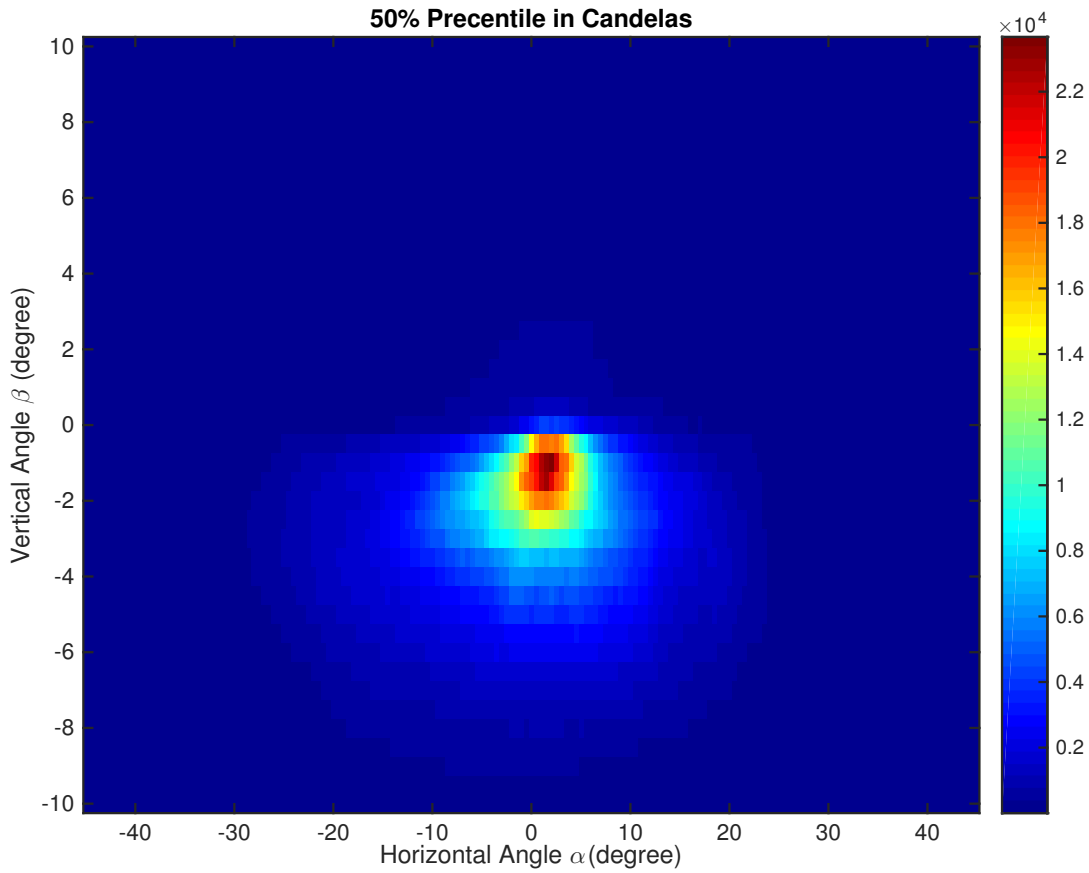

Figure 4.1: Isocandela ($I(\alpha, \beta)$)of the road surface from a pair of low beam headlamp luminous intensities at the 50th percentile, lamp height 0.66 m lamp separation 1.2m (Figure plotted using data obtained from [5]).

$$P_r = P_{LOS} + P_{NLOS} \tag{4.1}$$

where P_{LOS} is the received power due to the line of sight component and P_{NLOS} is the received power due to road surface reflections. The power received from road surface reflections can be blocked using a "space filter" installed on the photo-diode receiver.

Figure 4.2 depicts the framework for VLC calculations, where $I(\alpha, \beta)$ is the luminous intensity (cd), α and β are the horizontal and vertical angle with respect to the headlamp axis respectively. The received signal consists of line-of-sight component and non line of sight component and noise.

The LOS component P_{LOS} is calculated from the following equation.

$$P_{LOS} = \begin{cases} \dfrac{I_{LOS}(\alpha, \beta)}{LER \times r^2} A_r \cos(\theta_{LOS}) & 0 \leqslant \theta_{LOS} \leqslant \Psi \\ 0 & \theta_{LOS} \geqslant \Psi \end{cases} \tag{4.2}$$

Where r is the distance between the tail-light and the car behind, θ_{LOS} is the angle between the detector surface normal and the LOS incident direction, A_r is the detector area (see Figure 4.2) and Ψ is the field-of-view of the photo detector. In this channel model, the low-beam headlight is accurately modeled before it is scaled down to mimic the tail-light. The use of a high power phosphor-coated white LED with luminous efficacy of radiation (LER) 250.3 lm/W[6] is assumed.

The non-line of sight component (NLOS) is more computationally expensive to calculate (Figure 4.2) [133] . The NLOS component is calculated by dividing the road distance between with the two cars into many small patches (denoted dS Figure 4.2) and treating each patch as a secondary emitter[6]. The total reflected light power

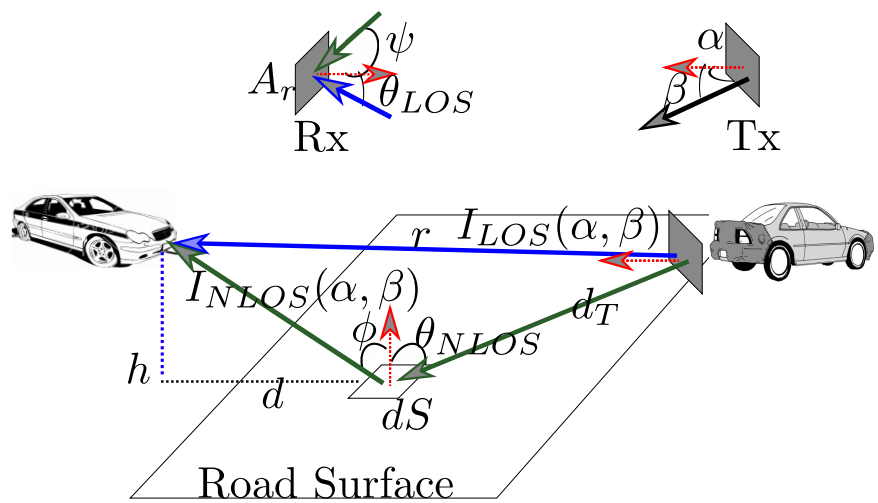

Figure 4.2: Framework for VLC calculations (based on [6])

from the road surface is then calculated at the receiver. Consider a given patch (dS) illustrated in Figure 4.2 then calculate the reflected light power from the road surface.

Repeatedly applying LOS model (Eq. 4.2) over patches dS to calculate the radiant flux received at the road integral square is given by:

$$dP_{NLOS} = \frac{I_{NLOS}(\alpha, \beta) \cos \theta_{NLOS}}{LER \times d_T^2} dS \tag{4.3}$$

Where θ_{NLOS} is the angle between the road surface patch (dS) normal and the NLOS incident direction and d_T is the distance between the tail-light transmitter and the road surface patch Figure 4.2. The road surface reflectivity (ρ) is modeled as a first order Lambertian diffuser with diffuse reflectivity $\rho = 0.4$ and a reflected radiant intensity $R(\phi)$:

$$R(\phi) = \rho \frac{\cos \phi}{\pi} \tag{4.4}$$

Where ϕ is the polar angle of the scattered light.

And the received optical power from one reflected path at the photodetector located in the car behind is:

$$dP_{NLOS} = \frac{I_{NLOS}(\alpha,\beta)\cos\theta_{NLOS}A_r.\rho\cos\phi\cos\psi}{LER \times \pi d_T^2.(d^2+h^2)}dS \tag{4.5}$$

Where h is the photodetector height and d is its distance from the road surface patch (dS). The total received power from all the illuminated area on the road is given by:

$$P_{NLOS} = \begin{cases} \iint_S \frac{I_{NLOS}(\alpha,\beta)\cos\theta_{NLOS}A_r.\rho\cos\phi\cos\psi}{LER \times \pi d_T^2.(d^2+h^2)}dS & 0 \leqslant \psi \leqslant \Psi \\ 0 & \psi \geqslant \Psi \end{cases} \tag{4.6}$$

where the P_{NLOS} integral is calculated assuming the road surface is a rectangular flat surface with no road surface irregularities. The integration over dS is bounded by the road surface between the two vehicles and a width of 6 meter.

The noise is modeled as thermal noise and shot noise which originates from background solar radiation and artificial light such as street light, advertising screens. The noise is modeled as additive white Gaussian noise (AWGN) with noise variance (parameters are calculated according to Table 4.1[6]).

$$\begin{aligned} \sigma_{total}^2 &= \sigma_{shot}^2 + \sigma_{thermal}^2 \\ \sigma_{shot}^2 &= 2q\gamma P_r B + 2qI_{bg}I_2B \\ \sigma_{thermal}^2 &= \frac{8\pi kT_k}{G}cAI_2B^2 + \frac{16\pi^2 kT_k\Omega}{g_m}c^2A^2I_3B^3 \end{aligned} \tag{4.7}$$

Table 4.1: Visible Light Communication Channel Model Parameters (taken from [6]).

Paramater	Symbol	Value
Diffuse reflectivity	ρ	0.4 [134]
Photo detector area	A_r	$1cm^2$
Order of Lamertian Diffuser	m	1
Luminous efficacy of radiation	LER	250.3 lm/W
FOV of the PD	Ψ	30°
Electronic Charge	q	1.6×10^{-19} C
Responsivity of PD	γ	0.54 A/W [135]
Received background noise current	I_{bg}	5100 μ A [135]
noise bandwidth factor for the background noise	I_2	0.562 [135]
noise bandwidth factor	I_3	0.0868 [135]
Boltzmann's Constant	k	1.38×10^{-23} J/K
Absolute temperature	T_k	298 K
Open-loop voltage gain	G	10 [135]
Fixed capacitance of PD per unit area	c	112 pF/cm^2 [135]
FET channel noise factor	Ω	1.5 [135]
FET transconductance	g_m	30mS [135]
System bandwidth	B	2 MHz

Weather conditions are represented by an additional path loss of 0 dB/km for clear weather and for fogy weather, studies [136][137] showed its $\approx$ 200 dB/km in low visibility conditions . The channel model is given by [138]

$$y(t) = \gamma x(t) * h(t; Tx, Rx) + n(t) \tag{4.8}$$

where $y(t)$ is the received signal, γ is the photodetector responsivity with units of $A/watts$ (Table 4.1), $h(t; Tx, Rx)$ is the channel impulse response, $x(t)$ is an on-off keying (OOK) modulated transmitted optical power in watts (Figure 4.1) and $n(t)$ is a AWGN noise with zero mean and spectral density given by equation 4.7.

The channel impulse response is given by [138]

$$h(t; Tx, Rx) = h^{(0)}(t; Tx, Rx) + h^{(1)}(t; Tx, Rx) \tag{4.9}$$

where $h^{(0)}(t; Tx, Rx)$ is the LOS response between transmitter and the receiver, $h^{(1)}(t; Tx, Rx)$ is the NLOS impulse response calculated from the LOS component [138] as

$$h^{(1)}(t; Tx, Rx) = \iint_S h^{(0)}(t; Tx, dS) * h^{(0)}(t; dS, Rx) dS \tag{4.10}$$

where $h^{(0)}(t; Tx, dS)$ is the channel impulse response from the transmitter to point dS and $h^{(0)}(t; dS, Rx)$ is the channel impulse response from point dS to the receiver. In this work the road surface is assumed to be a flat surface, such that light reflections from any road surface irregularities (e.g. speed bumps and road holes) are not considered.

The received power is given by [138]

$$P_r = H(0) \times \frac{I(\alpha, \beta)}{LER} \tag{4.11}$$

where $H(0)$ is the channel dc gain defined as $H(0) = \int_{-\infty}^{\infty} h(t; Tx, Rx) dt$ [138] .

In order to not reduce the light lifetime, OOK is employed with small modulation depth. Therefore, modulation depth of 20% is employed. The power level in the on time of the lamp is 110% of the nominal lamp power and the off time is 90% of the nominal lamp power. The low-beam head light power is $\approx$ 50 watts, which draws 4.5 amperes however the tail-light power is $\approx$ 25 watts, which draws 2.25 amperes. Modulation depth Δ of 20% for the tail-light power was chosen based on the currently available power amplifiers that can modulate 450 mA [139]. Increasing the modulation depth Δ can improve the results if the appropriate technology is

available in the future.

Define SNR as:

$$SNR = \frac{(\gamma P_r)^2}{\sigma_{total}^2} \tag{4.12}$$

Where γ is the photo detector responsivity and σ_{total}^2 is defined in equation 4.7. The corresponding bit error rate (BER) [6] is:

$$BER = Q(\Delta\sqrt{SNR}) \tag{4.13}$$

Where Δ is the modulation depth and $Q(x)$ is the Q-function used to calculate the tail probability of the standard Gaussian distribution and its given by

$$Q(x) = \frac{1}{\sqrt{2\pi}} \int_x^\infty \exp^{-\frac{y^2}{2}} \, dy \tag{4.14}$$

Figure 4.3 depicts the BER and the packet error rate of 100 byte packet length, at different weather conditions.

4.3 Performance Results

In this section the vehicular traffic simulation results for the VLC model presented in section 4.2 are quantified.

Similarly as in Chapter 3 the impact of the CV FCW on traffic safety is assessed. Simulations for different CVs market penetration rate are executed. For each communication model CV market penetration pair, 25 independent vehicular traffic simulation iterations are completed by my colleague Wade Genders.

The simulation results for the hybrid CV in a vehicular traffic network

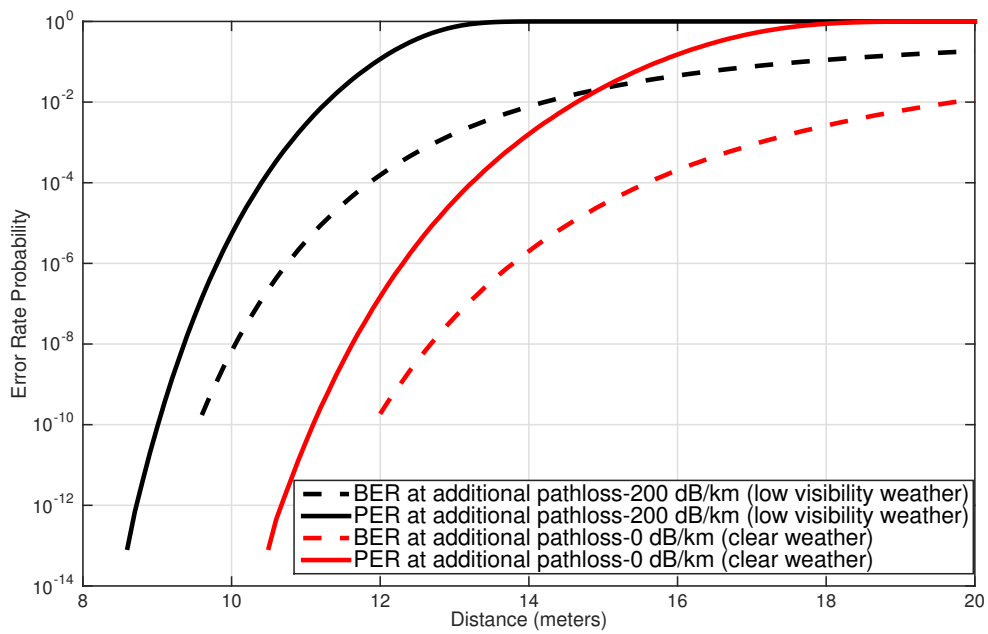

Figure 4.3: Visible light communication link error performance in different weather conditions

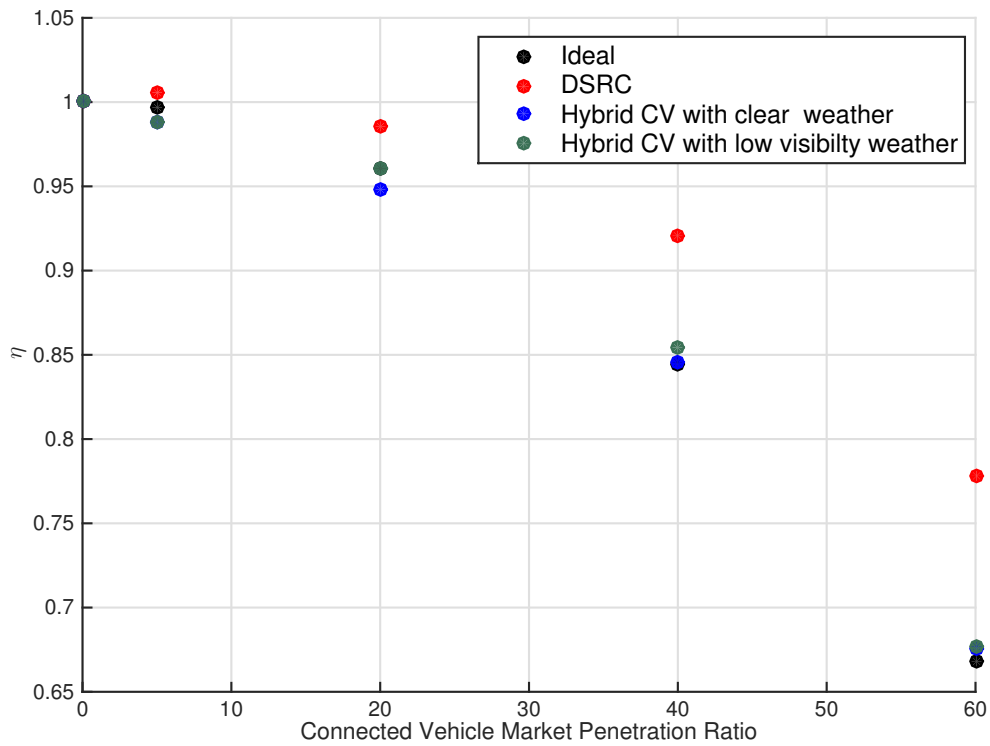

Figure 4.4: Variation of η over CV market penetration. The results in this figure is my colleague Wade Genders contribution based on DSRC and VLC channel models as an input to the vehicular traffic simulator.

performed by my colleague Wade Genders is displayed in Figure 4.4. The simulation results of a hybrid CV that is DSRC and VLC enabled is presented in different weather conditions. Research have found that VLC is resilient to weather conditions specifically in the forward collision warning application as the CVs separation distances in this specific scenario is small. Figure 4.5 presents the distance CDF distribution when a FCW is issued, with 70% of the FCW issued at distances below 10 meters. At connected vehicles market penetration ratio higher than 60% the DSRC performance improvement is expected to saturate and the performance of the Hybrid CV to continue to improve beyond the DSRC only case.

At 5% market penetration, there does not exist a difference between DSRC and hybrid η means, however at 20%, 40% and 60% the means are significantly different. The DSRC CVs are outperformed (i.e. exhibit a lower η) by the hybrid DSRC-VLC CVs at market penetrations above 20%. This indicates that there exists a critical market penetration between 5% and 20% where DSRC communication begins to degrade and the hybrid vehicles equipped with VLC V2V capabilities achieve higher communication rates. Hybrid CVs improves the vehicular network safety by 11% at CV market penetration of 60%.

4.4 Conclusion

Introducing visible light communications in vehicular communication has a potential to improve the performance in terms of communications reliability. A comprehensive visible light communication model in a vehicular environment was presented. The BER performance of the VLC model is characterized at different weather conditions. The visible light communication model was integrated in a vehicular traffic simulator

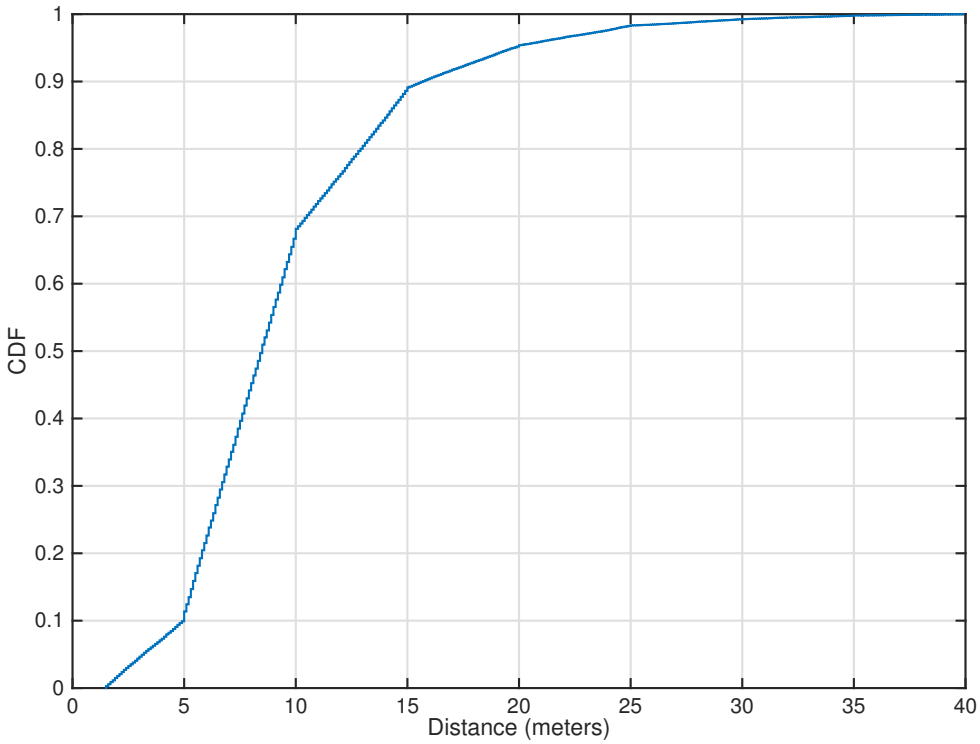

Figure 4.5: Distance CDF distribution when a FCW is issued. The data used to generate this CDF is obtained from the vehicular traffic simulator by Wade Genders.

to quantify the performance impact in realistic vehicular traffic environment.

Research has found that at market penetrations above 20%, CVs using DSRC communication experience significant communication degradation. This communication degradation leads to higher number of forward collision safety hazards involving a leading and following vehicles did not receive a FCW due to lost DSRC packets. Such an issue can be addressed by a hybrid DSRC-VLC communication method. A hybrid DSRC-VLC based FCW can decrease the total number of *critical TTC events* by 11% at market penetrations 60% .

Chapter 5

Multiple-Input / Multiple-Output Camera Communication (MIMO CamComm)

5.1 Introduction

Chapter 3 and Chapter 4 quantified communication channel BER performance for DSRC and visible light communication using photodetector as a receiver. The communication channel performance effect on a realistic vehicular traffic network was studied. Camera communication is another form of visible light communication utilizing a camera as a receiver instead of photodetector. Camera communication receiver provides an additional feature of visible light communication on top of imaging. Camera communication is able to spatially separate and process different transmitter sources independently. Multiple LEDs source can be captured in the camera simultaneously.

In this chapter a visible light communication BER performance is quantified using a novel visible light communication receiver architecture, utilizing two low cost rolling shutter cameras. The receiver is capable of at most double the data rate compared with single camera receiver architecture.

Rolling shutter cameras do not expose the entire sensor simultaneously, but exposes different parts of the sensor in different points in time. The camera shutter traveling across the sensor, from top to bottom, exposing each part of the sensor for the same brief amount of time (pixel-line scanning time). But, since the shutter is traveling, the top part of the sensor and the bottom part of the sensor are capturing different moments in time. The total scanning time for each row is the same and the delay between the rows is constant and depends on the camera read-out time, this is quantified in the camera specifications as camera line scanning frequency. A detailed timing diagram for the rolling shutter camera scanning is presented in Section 2.3. Although this behavior might seem undesirable specially in fast changing scenes, however this rolling shutter undesired behavior is utilized to transmit and receive digital data.

Utilizing the camera image sensor spatial diversity, a system data rate performance gain of at most double is achievable compared with the case of using one rolling shutter camera. The system performance gain is achievable for $2^i \times 2^i$ LED array of transmitters and two orthogonal rolling shutter cameras as a receiver. This performance gain is achievable only when the two cameras are organized as follows: the two cameras placed orthogonal to each other and are synchronized, such that at a specific sampling instant one camera scans the rows of the image and the other camera scans the columns of the same image.

In this chapter, the achievable receiving capabilities of the commercial rolling shutter camera is increased without hardware modifications. The reminder of this chapter is organized as follows, Section 5.2 presents the transceiver architecture, Section 5.3 depicts the simulation channel model. Section 5.4 depicts the performance of the system in different simulation setup. Section 5.5 describes the experimental setup. Finally, Section 5.6 concludes the chapter.

5.2 Communication System Model and Transceiver Structure

This section describes the communication system model. Two orthogonal rolling shutter cameras are used as the receiver and an array of LEDs as the transmitter. The transmitter is arranged in a square matrix, each LED is an independent transmitter source transmitting independent bit streams.

Figure 5.1 depicts the receiver architecture. The receiver consists of two synchronized rolling shutter cameras orthogonal to each other with a horizontal separation distance. The cameras separation distance results in a horizontal shift in the two images, this shift is called image disparity which could be utilized for stereo vision and localization applications. Image disparity means that there is pixel difference or motion between a pair of stereo image [117]. Image disparity and stereo vision were explained in more details in Section 2.3.1.

The orthogonality between the cameras results in the first camera scanning the first row of the scene, the second camera is scanning the first column of the same scene.

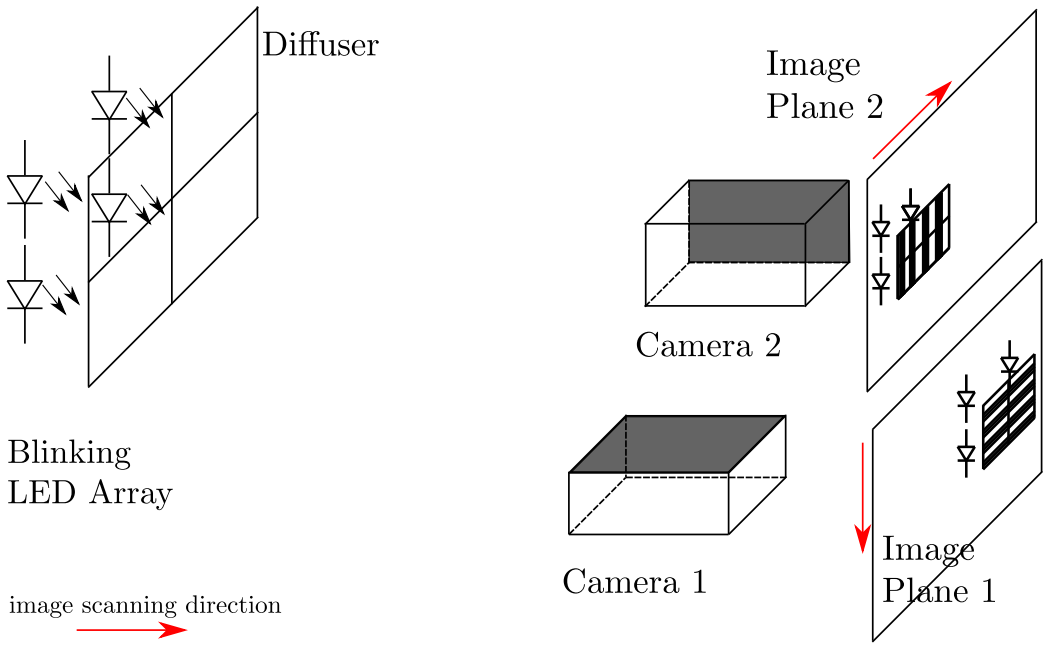

Figure 5.1: MIMO Camera Communication System Model.

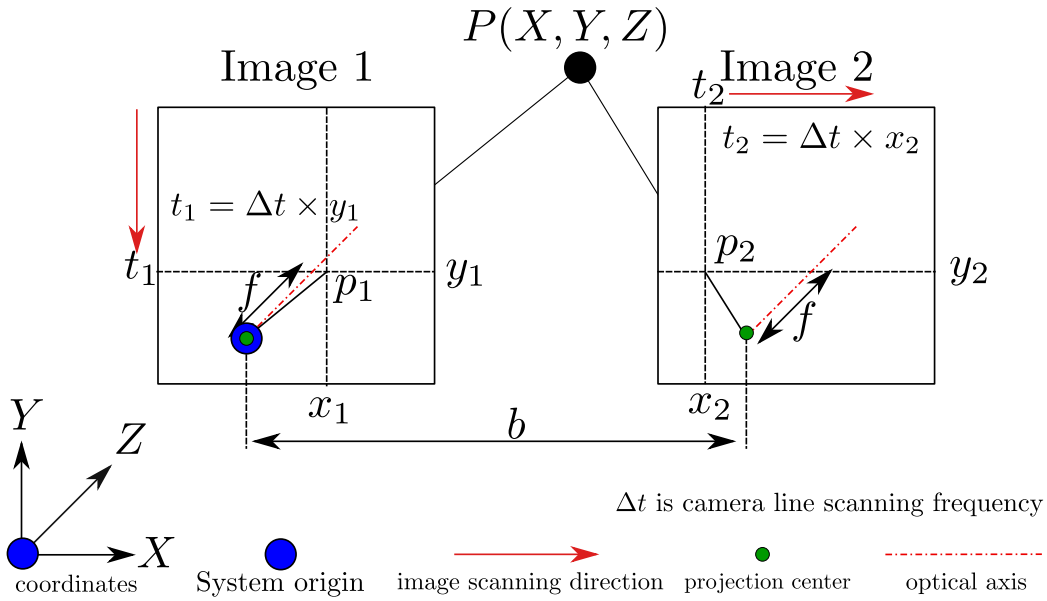

Figure 5.2: MIMO Camera Communication Mathematical Model.

Figure 5.2 depicts a mathematical model for the received images from the two cameras. A scene point $P = (X, Y, Z)$ is projected to an image point $p_1 = (x_1, y_1)$ and $p_2 = (x_2, y_2)$ in the two cameras respectively. The two projection centers are b distance away (which is the distance between the two cameras)

The cameras are synchronized in time (with each other and the transmitter) and orthogonal on each other and the optical axises with no tilting. A synchronization preamble is one way to achieve the transmitter receiver synchronization [140]. A periodically repeated idle pattern is continuously transmitted is another form of synchronization [141].

Orthogonal XYZ coordinate system is assumed, focal point (projection center) lies in the XY plane (cameras image plane). The focal length f is the cameras' focal lengths which defines the XY image plane in the XYZ coordinate system. The Z-axis is defined to be the optical axis of the camera and directed at the space of the scene. A camera projects scene point $P(X, Y, Z)$ into image points p_1, p_2 on two different cameras respectively.

The XYZ coordinate system origin coincides with the focal point of the first camera. The focal point of the second camera is located at distance b on the X axis $(b, 0, 0)$. Both cameras have the same focal length f with a parallel optical axes. The second camera is 90° rotated relative to the first camera thus the scanning in the second camera happens on the y-axis unlike the first camera where scanning happens on the x-axis.

From the ray theorem of geometry [118] and assuming a focal point equal projection center and optical axis coincide with Z-axis, therefore

$$\begin{aligned} p_1 = (x_1, y_1) = (\frac{fX}{Z}, \frac{fY}{Z}) \\ p_2 = (x_2, y_2) = (\frac{f(X-b)}{Z}, \frac{fY}{Z}) \end{aligned} \tag{5.1}$$

The point in the images are sampled at time t_1 and t_2 respectively. While the first camera is scanning on Y-axis direction for a point $p_1 = (x_1, y_1)$ is sampled at $t_1 = \Delta t \times y_1$ where Δt is the camera line scanning frequency. The second camera is scanning on the $X-$axis direction, for a point $p_2 = (x_2, y_2)$ sampled at $t_2 = \Delta t \times x_2$ since $y_1 = y_2$ therefore for any point on the second image where $x_2 \neq y_2$ there is a corresponding point on the first image sampled at different time instant.

Every sampling instant , each camera samples 2^i LEDs with an output of 2^i bits from each camera. The achievable data rate is at most doubled for every LED by using the second orthogonal camera with at most total system gain of $200 \times 2^i \times 2^i\%$ for an $2^i \times 2^i\%$ LED array compared with when using only one camera as a receiver.

Figure 5.3 depicts the transceiver block diagram, where the MIMO transceiver can be used for transmit multiplicity to improve the bit error rate performance (reliability) or for multiplexing to increase the transmitted data rate. A serial data stream is encoded then converted to parallel stream using serial to parallel converter with parallel output of $2^i \times 2^i$ unique streams those streams are mapped to $2^i \times 2^i$ LED transmitters. The receiver is two orthogonal synchronized rolling shutter cameras taking pictures of the same scene at the same time. The captured images are sampled, and an optimum detection threshold is applied on the sampled data. Utilizing de-mapper and error correction decoder data is received.

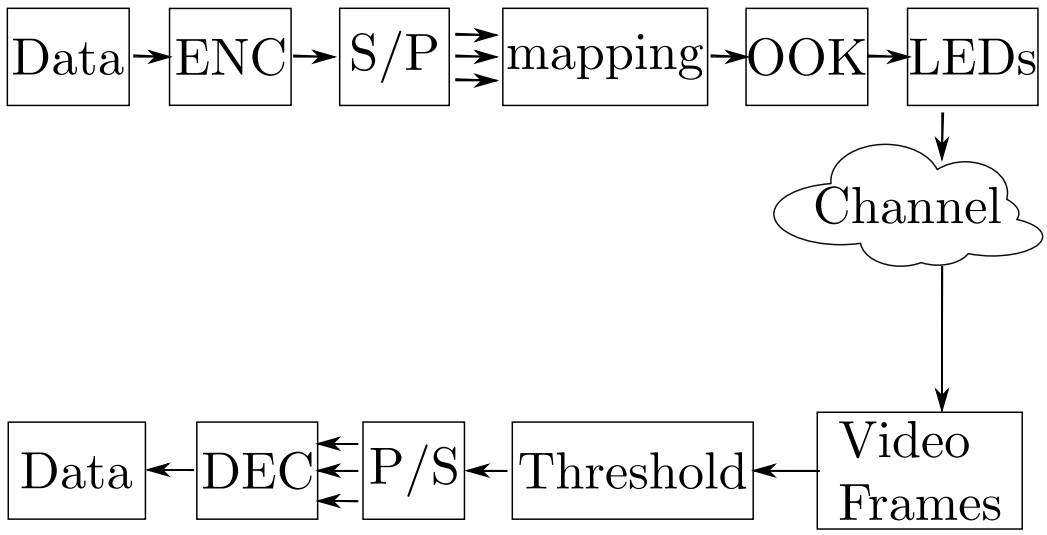

Figure 5.3: Rolling Shutter Camera Communication Transceiver Architecture

The rest of this section describes in detail the proposed transceiver architecture and the channel model.

5.2.1 Transmitter

The transmitter starts the data transmission message then it encapsulate the raw data using Reed Solomon coding to overcome the erasure channel effect. Figure 5.4 depicts an example for a blinking LED in an image taken by a rolling shutter camera to illustrate erasure channel concept. The LED transmits continuously during the entire image scanning time, however the camera receives data from the LED during the scanning time of the LED and all the data sent during T_1 and T_3 time slots are erased. The data erasure percentage is equal to the LED height in the image with respect to the entire image height or in other words the LED scanning time to the total image scanning time ($\frac{T_2}{T_1+T_2+T_3}$).

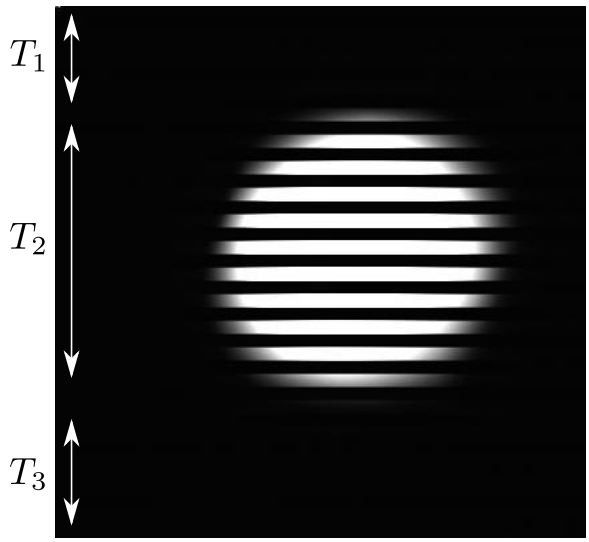

Figure 5.4: One LED Transmitter as perceived by rolling shutter camera

The transmitter is assumed to be an array of LEDs arranged in square matrix. Every LED is modulated using ON OFF keying (OOK), this is a simple visible light communication modulation form. The LEDs are turned on and off depending on the transmitted data where when the LED is on, its a logical transmitted one and when the LED is off its logic zero. Extinction ratio is defined as ratio between power level of logic zero to the power level of logic zero.

$$\text{Extinction ratio } \% = \frac{\text{logic 0 power level}}{\text{logic 1 power level}} \tag{5.2}$$

While the modulation is named ON-OFF keying, the "off" state can be not completely off but only light intensity (extinction ratio %) which is a system design parameter Figure 5.5. In both the experiment and simulation work in this thesis extinction ratio is 0%.

A camera system is a two-dimensional system, where the input light intensity to

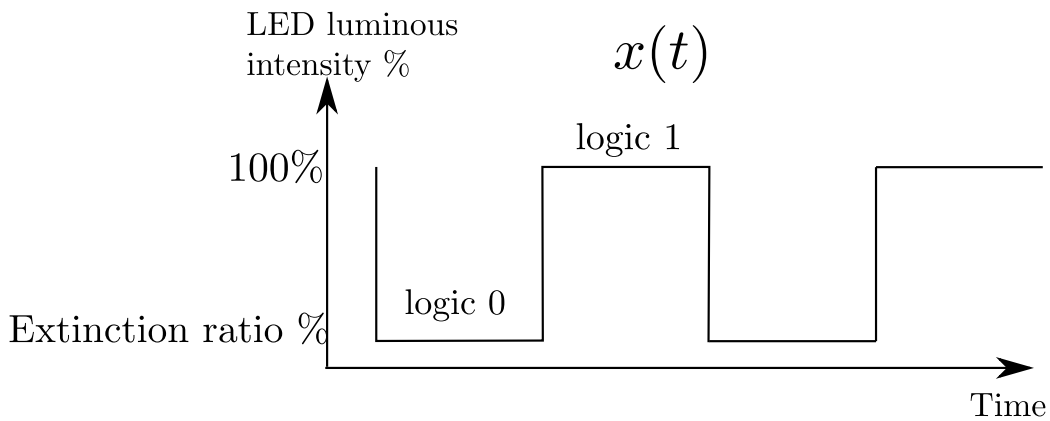

Figure 5.5: OOK Modulation

the camera is defined as a two dimensional function $f_1(x, y)$ and the output image light intensity is governed by $f_2(x, y)$. The relationship between the input and output is

$$f_2(x, y) = \iint_{-\infty}^{\infty} h(x, y; x', y') \; f_1(x', y') \; dx' \; dy', \tag{5.3}$$

where $h(x, y; x', y')$ is the camera spatial impulse response which represents the effect of the input at point (x', y') on the output at the point (x, y) also known as *point-spread function*.

Figure 5.6 depicts an object placed in a plane at distance d_1 from the camera lens and the image is formed at d_2 from the lens. The illumination field at the object is $U_1(x_1, y_1)$ using Frensel diffraction [7] the light field before the lens is given by

$$U_2(x_2, y_2) = \frac{i \exp(-ikd_1)}{\lambda d_1} \iint_{-\infty}^{\infty} U_1(x_1, y_1) \exp\left(- \frac{ik}{2d_1}\big((x_2 - x_1)^2 + (y_2 - y_1)^2\big)\right) dx_1 \; dy_1 \tag{5.4}$$

where λ is the light wave length and the k is the wave number given by $2\pi/\lambda$ and

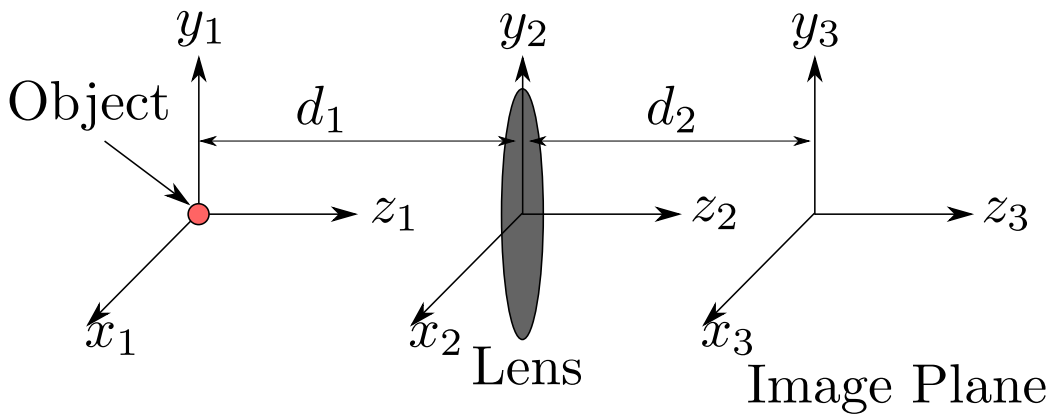

Figure 5.6: Coordinate systems to analyze the imaging performance [7]

i is $\sqrt{-1}$. For a lens with transmittance [7] of

$$t(x,y) = P(x,y)\exp\left(\frac{ik(x^2+y^2)}{2f}\right) \tag{5.5}$$

where f is the lens focal length and $P(x,y)$ is called the pupil function and it is the function responsible for the amplitude change in the incident light therefore the light field immediately after the lens is

$$\begin{aligned} U_2(x_2,y_2) =& \frac{i\exp(-ikd_1)}{d_1\lambda}P(x_2,y_2)\exp\left(\frac{ik}{2f}(x_2^2+y_2^2)\right) \\ & \iint_{-\infty}^{\infty} U_1(x_1,y_1)\exp\left(-\frac{ik}{2d_1}\left((x_2-x_1)^2+(y_2-y_1)^2\right)\right)dx_1\ dy_1 \end{aligned} \tag{5.6}$$

And the light field on the image plane [7] is given by

$$
\begin{aligned}
U_3(x_3, y_3) = & \frac{\exp\Big(-ik(d_1+d_2)\Big)}{d_1 d_2 \lambda^2} \iiiint_{-\infty}^{\infty} P(x_2, y_2) U_1(x_1, y_1) \\
& \exp\Big(\frac{ik}{2f}(x_2^2 + y_2^2)\Big) \exp\Big(-\frac{ik}{2d_1}\big((x_2-x_1)^2 + (y_2-y_1)^2\big)\Big) \\
& \exp\Big(-\frac{ik}{2d_2}\big((x_3-x_2)^2 + (y_3-y_2)^2\big)\Big) dx_1 dy_1 dx_2 dy_2
\end{aligned}
\tag{5.7}
$$

The intensity observed in the image is the modulus square of equation 5.7 [7]. Due to the complexity of equation 5.7, in this thesis the camera captured LED brightness pattern is modeled as a raised cosine. The raised cosine parameters are obtained utilizing *Point Grey Flea3 1.3 MP Mono USB3* camera measurements. A picture of the transmitter LED was captured and then a raised cosine pulse was fitted on the captured image. Figure 5.7 depicts the LED raised cosine pattern ($RC(x, y)$), in this model, the raised cosine roll-off factor is considered $\beta = 1/3$, where x, y are the image coordinates. $RC(x, y)$ is given by

$$
RC(x,y) = \begin{cases}
1, & |x| \leqslant \frac{1-\beta}{2} \& |y| \leqslant \frac{1-\beta}{2} \\
\frac{1}{2}(1 + \cos\big(\frac{\pi}{\beta}(|x| - \frac{1-\beta}{2})\big) \times \frac{1}{2}(1 + \cos\big(\frac{\pi}{\beta}(|y| - \frac{1-\beta}{2})\big), & \\
\frac{1-\beta}{2} < |x| \leqslant \frac{1+\beta}{2} \& \frac{1-\beta}{2} < |y| \leqslant \frac{1+\beta}{2} & \\
0, & \text{otherwise}
\end{cases}
\tag{5.8}
$$

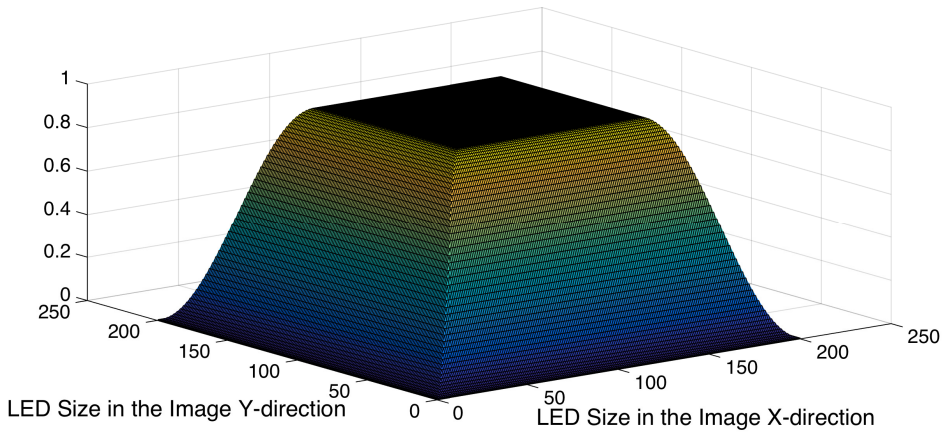

Figure 5.7: LED Raised Cosine Model Pattern ($RC(x, y)$) with roll-off factor $\beta = 1/3$.

5.3 Channel Model

Figure 5.8 depicts the camera channel model used in the simulations [8] . The camera digital sensor converts the photons hitting the pixel to a digital number through multiple steps. The camera exposes the sensor to the light for a certain duration of time named exposure time, after this exposure time certain number of photons hit the pixel of area A , a fraction of those photons creates electrons. This fraction is quantum efficiency ($QE(\lambda)$) and it is defined by

$$QE(\lambda) = \frac{\mu_{electrons}}{\mu_{photons}} \tag{5.9}$$

Where $QE(\lambda)$ is the camera quantum efficiency at the incident light wavelength (λ) , $\mu_{electrons}$ is the number of the generated electrons in the pixel, and $\mu_{electrons}$ is the number of photons hitting the pixel during a time of $t_{exposure}$ seconds. The number of electrons $\mu_{electrons}$ is random and has a Poisson distribution with mean $\eta\mu_{photons}$

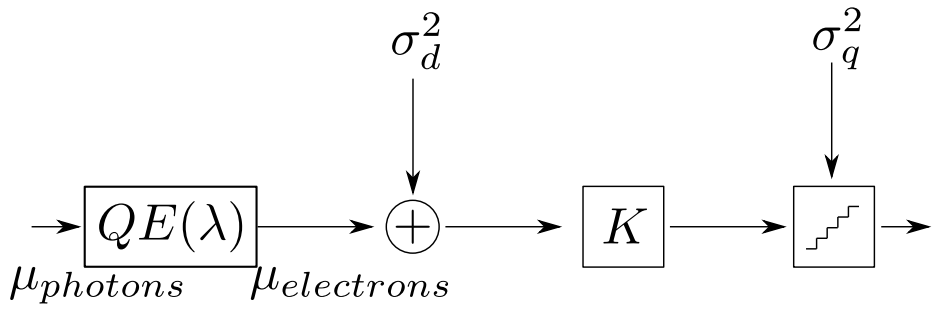

Figure 5.8: Physical and Mathematical model of a single Camera Pixel [8].

and variance $\eta\mu_{photons}$

The mean number of photons hitting the pixel $\mu_{photons}$ [8] is given by

$$\mu_{photons} = \frac{AEt_{exposure}}{hc/\lambda} \tag{5.10}$$

Where E is the irradiance on the sensor surface in W/m^2, $h = 6.62 \times 10^{-34}$ is Planck's constant and $c = 3 \times 10^8$ is speed of light.

Figure 5.10 depicts the brightness of one LED as received by the camera at different distances, the curve is calculated using practical measurements of a commercial philips light bulb (Philips Rebel LED lightbulb-6 LED round) at multiple operating distances and the rest of the curve is calculated using inverse square law where the light intensity is proportional to the inverse of square of the travelled distance. The lux measurements are compared against the simulated lux values in Figure 5.9 for a maximum distance of 0.6 meters due to lab distance constrains.

The value of irradiance in lm units is converted to watts unit by division by the conversion factor of 683 at operating light wave length $\lambda = 525$ nm [142], a more detailed description of radiometric and photometric units is discussed in Section 2.2.1.

The noise is modeled as signal independent and signal depended noise, the signal

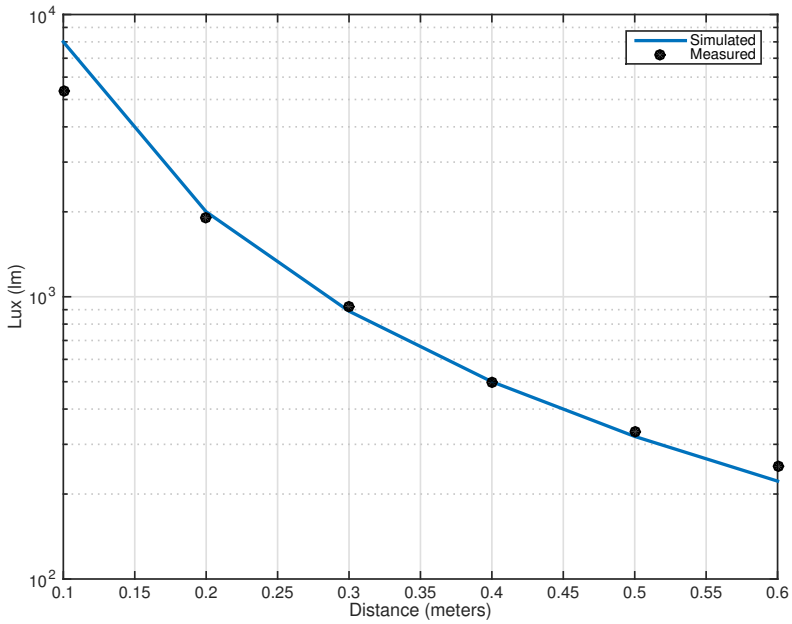

Figure 5.9: Measured LED lux brightness vs distance.

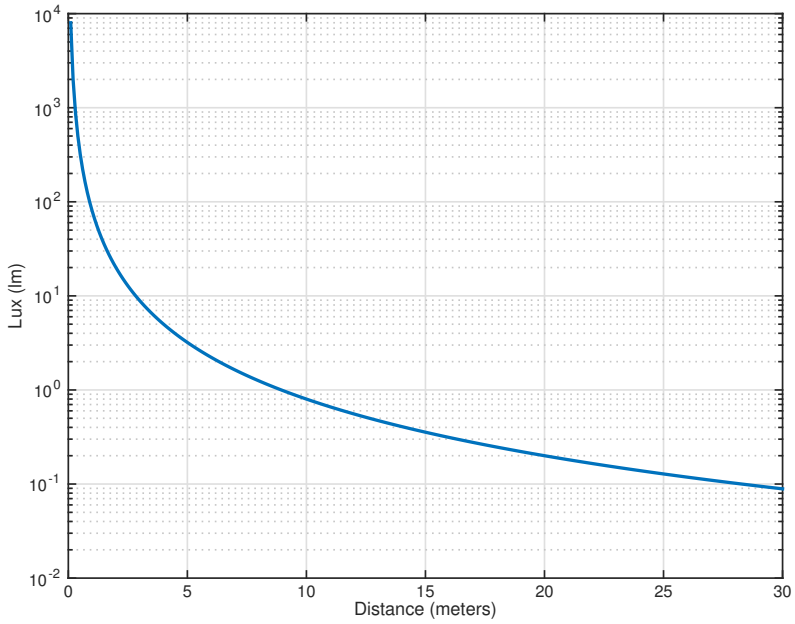

Figure 5.10: Simulated LED lux brightness (lm) vs distance (meters).

Table 5.1: Camera parameters obtained from *Point Grey Flea3 1.3 MP Mono USB3* camera specification document [10].

Parameter	Value
Pixel Area	$(3.63um)^2$
Exposure	1/120 seconds
Operating light wavelength (λ)	525 nm
Quantum efficiency QE at $\lambda = 525$nm	77%
σ_d^2	6^2
Gain (K)	3.7037

independent noise is divided into σ_q^2 and σ_d^2. The quantization noise is uniform-distributed with a variance of $\sigma_q^2 = 1/12DN^2$ [117] (DN is a dimensionless unit for count) and normally distributed dark noise with variance σ_d^2. The dark current noise (or read noise) occurs due to the energy arises in the sensor and the surrounding electronics [8], during the camera operation time random electrons are created that fall into the sensor wells which are detected and converted into signal without photons hitting the sensor.

And the signal dependent noise variance is $(K \times QE \times \mu_p)^2$, where K is the camera sensor gain. The SNR is defined as

$$\begin{aligned} SNR(\mu_p) &= \frac{\text{mean number of useful electrons}}{\text{mean number of noisy electrons}} \\ &= \frac{K \times QE \times \mu_p}{\sqrt{\sigma_d^2 + \sigma_q^2 + (K \times QE \times \mu_p)}} \end{aligned} \tag{5.11}$$

Figure 5.11 depicts the SNR versus distance is calculated based on the table 5.1, the utilized transmitter LED brightness level saturate the camera sensor well on distances less than 1 meter resulting in the maximum achievable SNR (41.9 dB) by the *Point Grey Flea3 1.3 MP Mono USB3* camera .

The total accumulated charge on the camera sensor is the sum of Poisson random

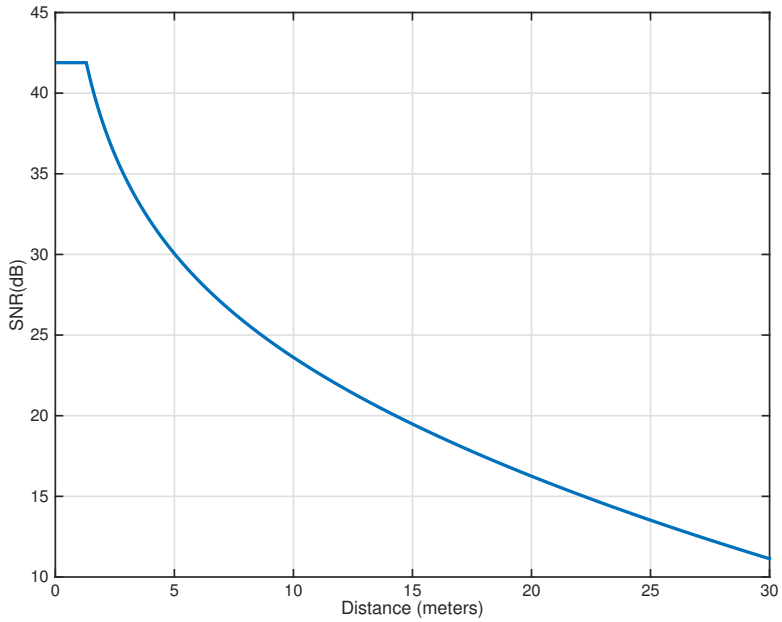

Figure 5.11: Rolling Shutter camera pixel SNR versus transmitter-receiver distance.

variable (the desired signal) and the independent random variables (noise), where the mean of total accumulated charge is given by

$$\mu = K \times QE \times \mu_{photons} \tag{5.12}$$

and all the noise variances adds up [8] therefore the variance of the received signal is given by

$$\sigma^2 = K^2(QE \times \mu_{photons} + \sigma_d^2) + \sigma_q^2 \tag{5.13}$$

The camera receiver detector measure the total charge and compares it to a predefined optimum threshold ϑ. To calculate the optimum threshold, the mean of the received signal is considered in case of a transmitted bit 0 and 1 respectively

$$\begin{aligned} \mu_0 &= 0 \\ \mu_1 &= K \times QE \times \mu_p \end{aligned} \tag{5.14}$$

And the variance is

$$\begin{aligned} \sigma_0^2 &= \sigma_q^2 + K^2\sigma_d^2 \\ \sigma_1^2 &= \sigma_q^2 + K^2\sigma_d^2 + K^2 \times QE \times \mu_p \end{aligned} \tag{5.15}$$

When bit 0 is transmitted, the received signal have dark noise component this signal is quantized in later stage in the receiver thus adding quantization noise component to σ_0^2.

The Poisson distribution of the received signal with variance $\sigma^2_{Poisson} = K^2 \times QE \times \mu_p$ and mean of $\lambda_{Poisson} = K^2 \times QE \times \mu_p$ can be approximated to a Gaussian distribution for sufficiently large $\mu_{photons}$ [143].

The optimum threshold ϑ is designed by intersecting two Gaussian distributions with means μ_0, μ_1 and variances σ_0^2, σ_1^2, as known by Maximum likelihood decoding [107].

The bit error when the transmitted bit is zero (p_0) is the integral of the Gaussian distribution of the σ_0^2 variance from ϑ to ∞ and the bit error when the transmitted bit is one (p_1) is the integral of the Gaussian distribution of variance σ_1^2 from $-\infty$ to ϑ. The optimum threshold minimizes $BER = \frac{1}{2}(p_0 + p_1)$.

The OOK modulation bit error rate is approximated as $BER \approx Q(\zeta)$ [144] as shown in Figure 5.12, where Q function is defined in equation 4.14. The BER is calculated assuming an optimum-threshold receiver where

$$\zeta = \frac{\mu_1 - \mu_0}{\sigma_0 + \sigma_1} \tag{5.16}$$

The LED size in the image is governed by the original physical parameters of the LED as well as the maximum desired system operating distance. The LED size in the image is governed by lens maker equation

$$h_i = \frac{f h_o}{d_o - f} \tag{5.17}$$

where h_i is the height of the object in the image, f is the lens focal length, h_o is the object size and d_o is the distance of the object from the camera. The number of the stripes depends on the ratio between the LED blinking frequency and the camera

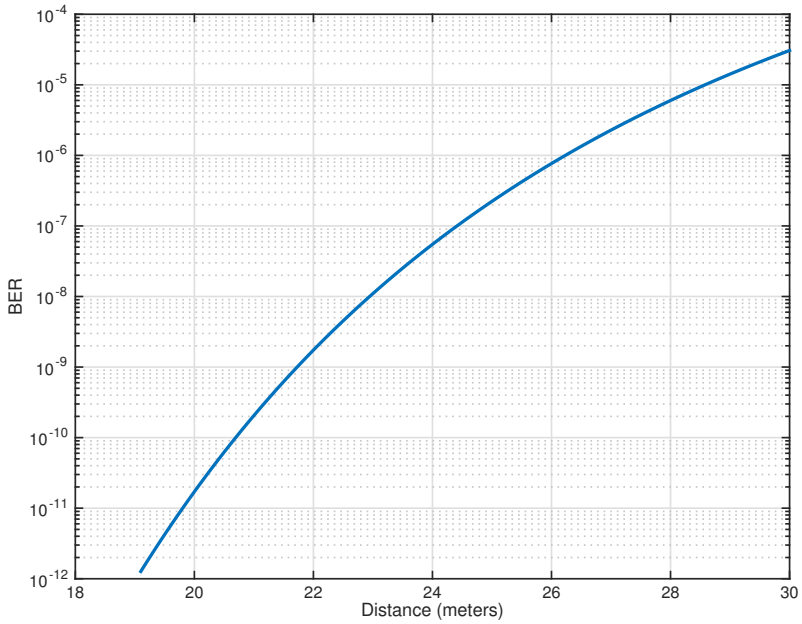

Figure 5.12: OOK modulated light bit error rate versus distance utilizing an LED with brightness depicted in Figure 5.10.

line scanning frequency as well as the LED image size. For example if this ratio is 5 that means that the width of every stripe is 5 pixels and depends on the LED height in the image then how many stripes are observed in one LED image.

5.3.1 Receiver

The camera image sensor achieves interference free communication in case of multi LEDs transmission, provided that the received LEDs are spaced in the received image without the need to complicated protocol stack unlike radio frequency communication.

In this work, camera communication data rate improvement utilizing inexpensive cameras and commercial LEDs is evaluated. The receiver consists of two synchronized rolling shutter cameras orthogonal to each other, such that when the first camera is scanning the first row the second camera is scanning the first column.

The receiver algorithm is simple, the camera starts by capturing a series of frames / video then assuming the usage of the image processing techniques to acquire and locate the LED and estimate its size. The receiver extracts a part of the image that contains the LED and start the decoding process. Figure 5.13 depicts the decoding process. Optimum threshold is utilized, a continuous bit sequence is converted into a single value by down sampling the data according to the bit stripe width. Received bits are collected in a symbol form. If the correctly acquired received data symbols are at least equal to k then Reed Solomon decoder is employed otherwise more frames are required to successfully decode the transmitted message.

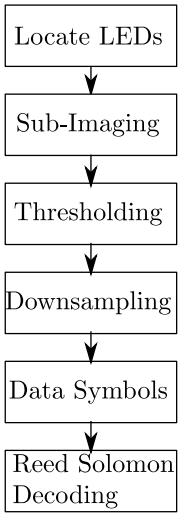

Figure 5.13: Decoder Flow Chart

System Code Rate Design

The design of the system coding rate is very crucial and it depends on the system channel. Reed Solomon code as a digital fountain code [108]. In a digital fountain code the transmitted data is recoverable once the receiver successfully receives at least the same amount of transmitted symbols. In this thesis, it is assumed that the receiver is able to locate the LEDs in the received images. However in practice, the location of the LED in the image can be obtained by subtracting consecutive frames to locate the modulated LEDs [97]. A different approach to locate the LEDs is discussed in [145] by using simple feature object detection.

The Reed Solomon code design parameters are m, n, k, where m is the symbol size, k is the number of data symbols being encoded, and n is the total number of code symbols in the encoded block with a maximum value $2^m - 1$ For the most conventional R-S (n, k) code.

The design of the RS coding rate depends on multiple factors namely: the LED

physical dimensions, the camera scanning line frequency, the LED blinking frequency, the maximum desired system operating distance and system latency.

The system is designed such that at least one symbol is correctly received for each LED every frame. Designing m depends on the maximum number of continuously received bits for every LED in one image, such that at least one symbol is received correctly with no bit erasures. The number of received bits for every LED varies depending on how the camera captures the LED in the image, namely the LED size in the image and how many stripes are there in the LED image.

The design of the Reed Solomon k value will affect the system latency, such that the decoder will start decoding once it correctly receives at least k symbols.

5.4 Simulation Results

The simulation setup consists of two orthogonal cameras models taking two images and sample them. The first camera capture an image of the LED transmitters, sample them horizontally. The second camera captures the image of the same scene at the same time but with 90° rotation, sampling on the rotated direction as well.

Table 5.2 presents the simulation parameters used in the simulator. The maximum image obtained from the two cameras is 640×640 pixels with LED blinking frequency 13.075 KHz. The utilized LED transmitter physical parameters have a 3 cm diffuser in-front of every LED and separation distance of 1 cm between the LED.

Figures 5.14 and 5.15 depict a 2×2 LED transmitter as it captured by the two camera receiver at different distances, while transmitting a sequence of all ones and ones-zeros sequence respectively. The yellow line in the image represents the actual image boundaries while the maximum size of the image is still displayed to show the

Table 5.2: MIMO CamComm Simulation Parameters

Parameter	Value
Image Dimensions	640×640 pixels
Line Scanning Frequency	1/130750.6 seconds
LED Blinking Frequency	1/13075 seconds
LED Diffuser Size	3 cms
LED Spacing	1 cm
Cameras separation distance	5 cm
Focal Length	5.3 mm

relative size at different distances. The figures show how the LED transmitter scales relative to the big image at different distances. The size of the transmitter LED, as well as the separation distances between them scales according to the lens maker equation (eq. 5.17).

In the simulation setup its assumed that the camera processes the image frames and start scanning the new scene with no gap in the scanning time before start scanning the next frame. However in real life cameras, the camera will be processing the previous image before start scanning the new one which results in timing gap between the time stamp of frame start scanning Figure 5.16.

The LED location in the image changes according to the lens maker equation. This location is translated into different samples in time, which means receiving different parts of the code words as the distance change.

A 100 independent Monte Carlo simulation with different seed for each Monte Carlo trial was executed to quantify the simulation performance.

Figure 5.17 depicts the data rate for every LED source utilizing one camera as a receiver. The capacity is defined as the total number of received non erased bits. The

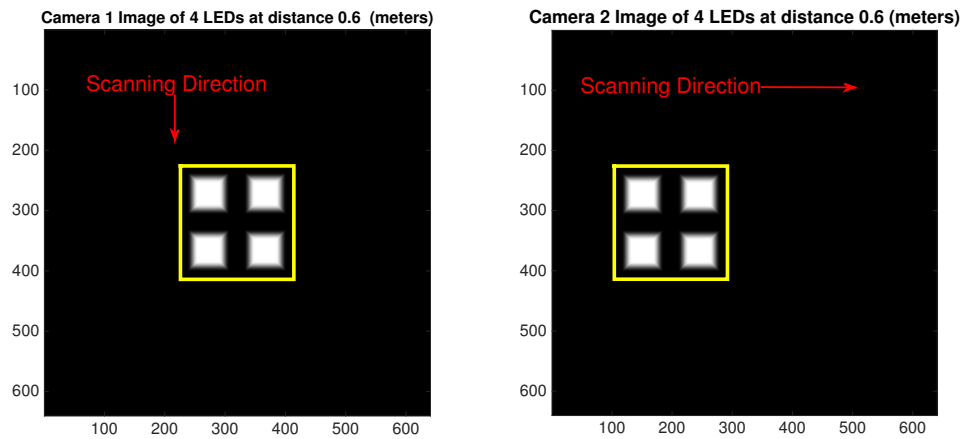

Figure 5.14: Simulated Image of 2×2 LED transmitter at distance of 60 cms, with all ones data sequence transmitted.

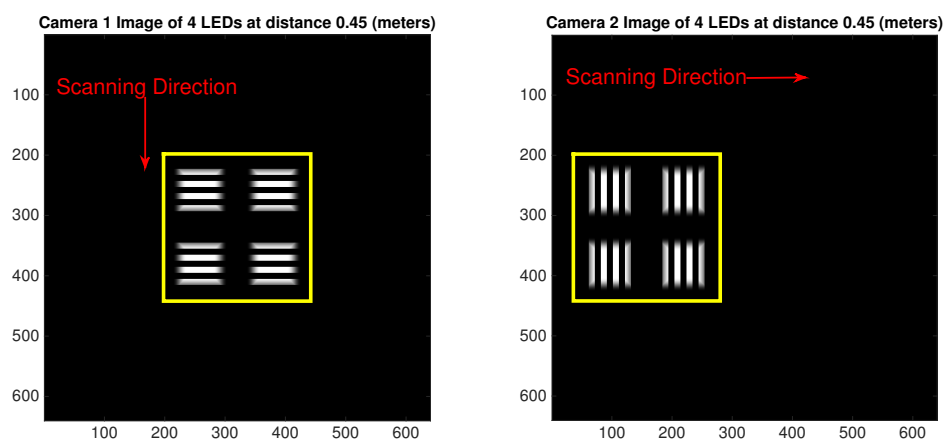

Figure 5.15: Simulated Image of 2×2 LED transmitter at distance of 45 cms, with ones-zeros data sequence transmitted.

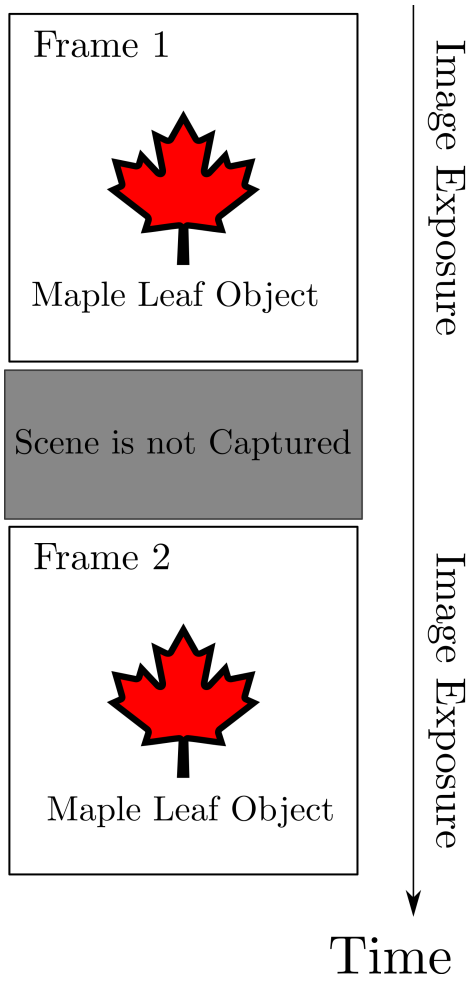

Figure 5.16: Camera Timing Diagram.

capacity is computed as follows

$$\text{Capacity} = \frac{h_i}{\text{LED Blinking Frequency/Line Scanning Frequency}} \tag{5.18}$$

where h_i is the LED size in the image in pixels units (defined in equation 5.17 in meters), LED Blinking Frequency and Line Scanning Frequency are given by table 5.2.

Various Reed Solomon coding rate was explored and the achievable data rate was quantified. For Reed Solomon Coding rate of 9/15 it utilize the non erased received bits in the most efficient way achieving the capacity value.

Figure 5.18 depicts the number of received bits at the MIMO CamComm receiver (2 cameras). The curves are normalized for every LED transmitter, in other words the received number of bits using one LED as a transmitter and two cameras as a receiver is 45 bits per-frame at transmitter-receiver inter-distance of 0.2 utilizing Reed Solomon code with coding rate of (9/15). A per LED data rate improvement of 200 % is achieved thus enables system performance gain of at most double for an LED transmitter of $2^i \times 2^i$ LEDs

5.5 Experimental Setup

In this section the setup used to validate the idea is presented. The commercially available LEDs (*Philips Rebel LED lightbulb (6 LEDs round)*) is utilized. The hardware for the transmitter was designed and implemented by Warren Pawlikowski. This included modifying the bulb, making the driving circuitry and interfacing the micro-controller boards.

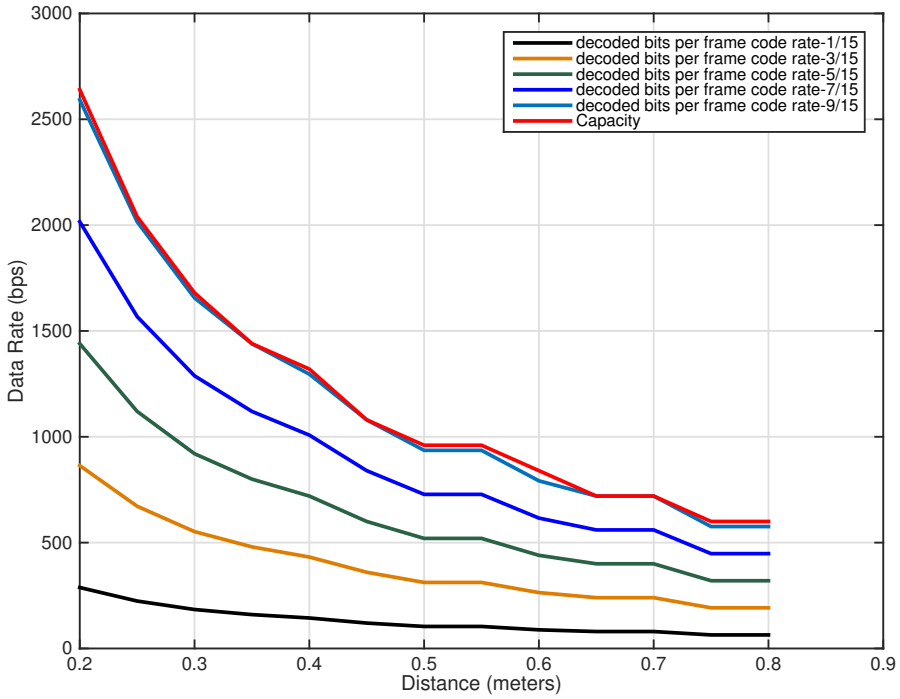

Figure 5.17: Simulated data rates for 2×2 LED transmitter for 4 bits symbol size for different RS coding rates using only one camera as a receiver.

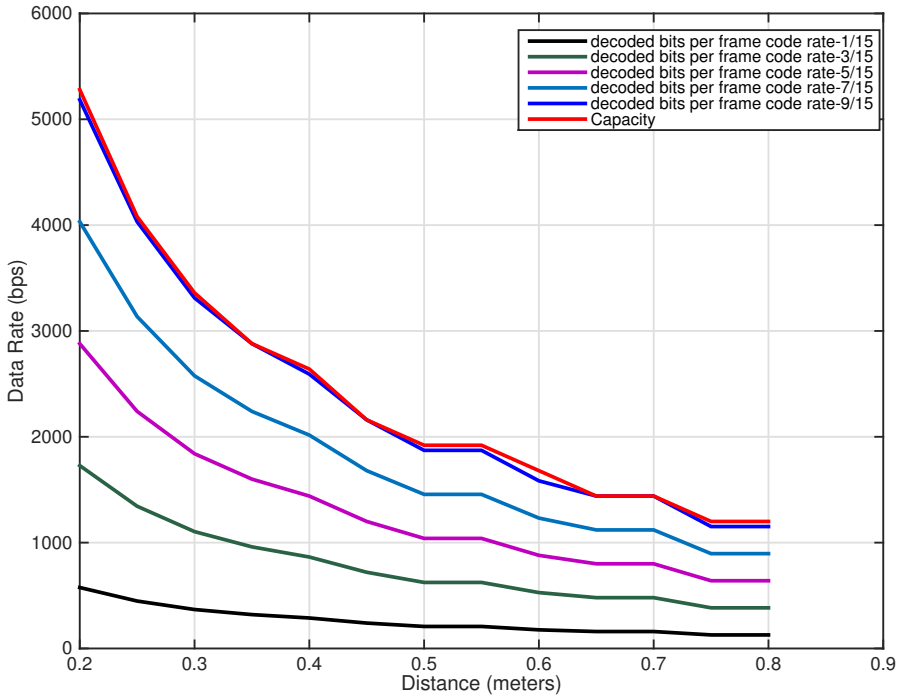

Figure 5.18: Simulated data rates for 2×2 LED transmitter for 4 bits symbol size for different RS coding rates using two cameras as a receiver.

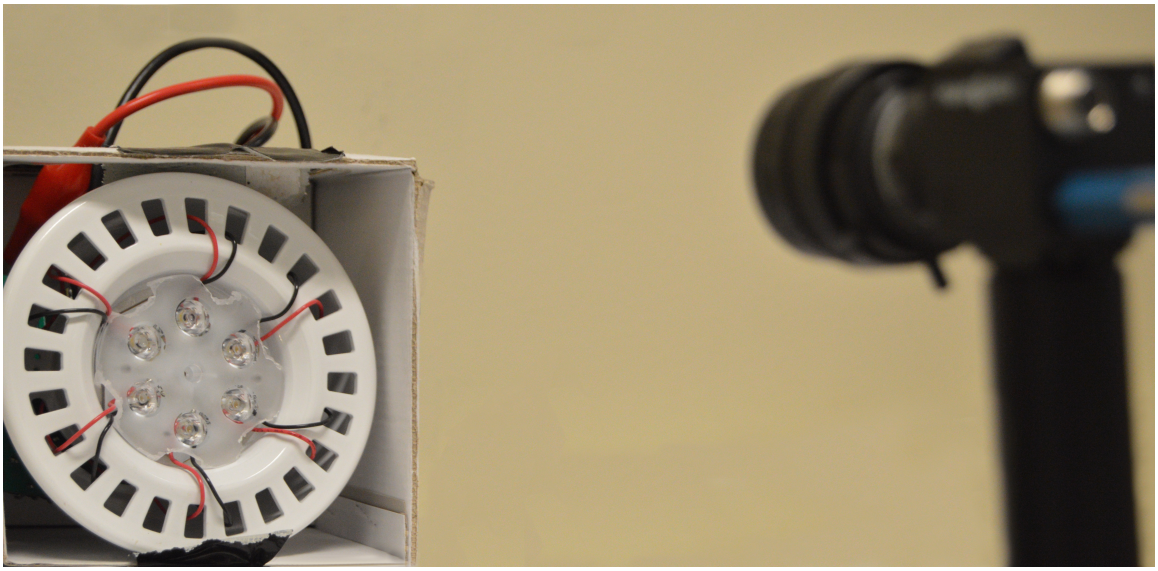

Figure 5.19: Experimental lab set-up. The light bulb on the left is a commercial light bulb modified by Warren Pawlikowski.

The setup consists of a commercial light bulb where LED is independently driven and controlled by different output pin from the Teensy 3.1 board. In the setup a 2×2 LEDs are utilized independently modulated from 4 different data sources. Figure 5.20 presents the assignment of the LED in the transmitted data frame, the top LED is sampled first in time and it represents the start frame delimiter (SFD) the middle 4 LEDs represent the useful data transmitted. The last sampled LED the one in the bottom of the image represents the End Frame Delimiter (EFD).

The SFD and EFD are using in the experiment setup for accurate synchronization between the transmitter LED luminary. A pre-determined pattern is sent on both the SFD and EFD LEDs and when the receiver detect the start and the end of the transmitted frame.

Figure 5.19 shows the experimental lab set-up, a rolling shutter camera is pointed

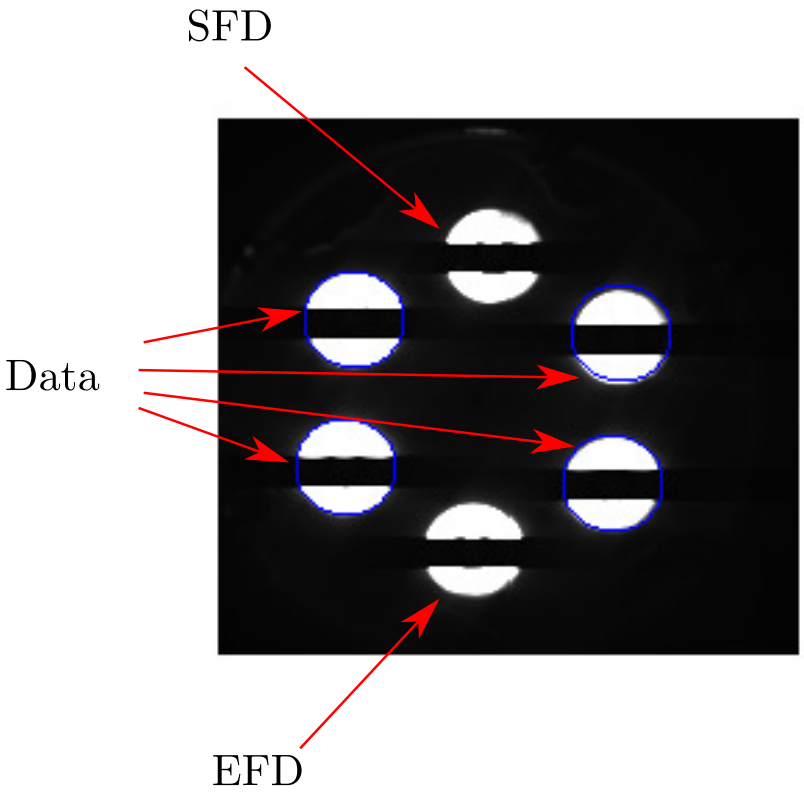

Figure 5.20: Luminary Architecture with LED assignment

directly in-front of the LEDs. The LED is modulated using a Teensy 3.1 controller and repeatedly transmit a data sequence. The LED transmitter is in focus 40 cms away from the camera. The location of the LEDs in the commercial Phillips bulb are not altered, approximately 1.1 cm diffuser and 1 cm spacing between the LEDs. The camera takes sequence of pictures/video which is processed by Matlab to successfully decode the transmitted data.

The experimental data results show a performance of data received from 4 data LEDs at distance of 40 cms over a duration of 2775 frames is 77700 bits with 0/77700 wrong bits , at a camera frame rate of 120 fps and the data rate of 3360 bps, with a per LED data rate of 840 bps. A capacity of 960 bps per LED is predicated by the simulator. The capacity is observed at 40 cms and at LED transmitter dimensions of 1.1 cm LED diffuser and 1 cm spacing. This experimental setup could be scaled up to be usable in connected vehicle applications with required operating distances of approximately 10 meters by utilizing different camera magnification and LED diffuser size. An example of the payload data to be transmitted between the vehicles is speed, engine revolution, brake status and turning signals [78].

Doubling the data rate is possible utilizing an orthogonal synchronized camera placed next to the first camera, taking an orthogonal video of the same scene at the same time with the LED sampled at different time instants leading to double of the data rate (eq: 5.1). Due to limited equipments this was only quantified using one camera.

5.6 Conclusion

This research found that there is a potential data rate gain of at most double is compared with one camera as a receiver case. This gain is achievable by utilizing two orthogonal rolling shutter cameras and commercial LEDs. This data rate gain claim was supported by a mathematical explanation as well as simulation results.

Using the single rolling shutter camera gives us (2^i) bits every sample instant using the same $2^i \times 2^i$ array of LEDs transmitters however the two rolling shutter cameras gives 2^{i+1} bits for every sampling instant using the same transmitter. The percentage gain the in data rate is $200 \times 2^i \times 2^i\%$ compared with when using only one camera as a receiver.

Future work include quantifying the impact of non perfectly orthogonal cameras in the receiver. Also relative receiver transmitter movement due to vehicle vibrations. As well as including more experimental measurements at different transmitter-receiver inter-distance. Using a secondary camera to capture LEDs and quantifying the data rate claimed in the simulation set-up.

Chapter 6

Concluding Remarks and Future Directions

6.1 Conclusion

Connected vehicles have the potential to improve transportation safety, mobility and sustainability through information sharing. Wireless communication via V2V DSRC can potentially benefit many connected vehicle applications, but understanding its limitations is important to optimizing its use. This research have found that at connected vehicle market penetrations above 40%, V2V DSRC performance degrades sharply. Many *critical TTC* situations involving a leading and following vehicle did not receive a FCW due to lost V2V DSRC packets. The potential improvements in mitigating rear-end collisions are large, as when simulating a perfect channel, an 33% reduction in rear-end collisions was observed. Other V2V communication methods that do not suffer when market penetrations increase should be the focus of future research. Visible light communications (VLC) is a potential candidate communication

technology which can succeed when DSRC performance degrades, retaining successful communication probability at high market penetrations. VLC is used in tandem with DSRC to improve the communication reliability in high market penetration rate. VLC improves the rear end collision warning with 11 % compared with DSRC only scenario at Connected Vehicle market penetration of 60%.

MIMO camera communications is also quantified in this work. An improvement of double the data rate is observed using two orthogonal synchronized cameras compared with one camera. A practical prototype is utilized to quantify the rolling shutter camera performance as visible light communication receiver. Practical measurements show a raw bit error rate of 0% measured at 40 cms over 2775 frames.

6.2 Future Directions

In Chapter 3 and 4 DSRC and VLC channel models are integrated in vehicular traffic simulator. Future directions includes adding more channel impairments to improve the channel model reliability. Specifically in the DSRC channel model detailed modeling of the interference channel instead of adding the interference as an additive white gaussian noise. Including DSRC MAC layer functionalities to improve the performance is also future direction.

For the VLC channel model presented in chapter 4 the BER was quantified for a scaled down version of low beam headlight pattern a future direction includes quantifying the BER performance for different lights in the vehicle, namely turn signal light and number plate light. Exploring an active system for example a LIDAR and compare it's performance with the visible light communication system.

Similar to University of Michigan driverless city where the university built a large

scale driverless city to quantify the impact Connected Vehicles in large scale realistic environment. A smaller test-bed could be utilized to evaluate the performance of the Connected Vehicles in specific realistic scenarios in collaboration with existing McMaster University automotive research center. A simple scenario of forward collision warning system could be an example.

In Chapter 5, a simulation setup was presented to quantify the camera communication data-rate performance. Future directions include simulating relative camera to the transmitter orientation as well as exploring a more accurate modeling of the LED pattern in the image.

In Chapter 5, a proof of concept experiment that enables rolling shutter camera as a receiver and commercial LED as a transmitter was presented. A synchronization between the transmitter and the receiver was achieved using 2 LEDs as a start-of-frame and end-of-frame. Future directions include exploring hardware triggered synchronization between the camera and the Arduino board to improve the reliability of the synchronization. Utilizing the camera communication setup for vehicle localization purpose. Furthermore, adding different impairments in the experimental camera setup namely non perfectly orthogonal cameras in the receiver as well as relative displacement between transmitter and receiver due to vehicle motion and different weather conditions.

Bibliography

[1] J. Kenney, "Dedicated short-range communications (DSRC) standards in the United States," *Proceedings of the IEEE*, vol. 99, no. 7, pp. 1162–1182, July 2011.

[2] Spectrum Management and Telecommunications, "Proposed spectrum utilization policy, technical and licensing requirements to introduce dedicated short-range communications-based intelligent transportation systems applications in the band 5850-5925 MHz," Industry Canada, Tech. Rep., March 2007. [Online]. Available: https://www.ic.gc.ca/eic/site/smt-gst.nsf/vwapj/consultation-shortrange-e.pdf/$FILE/consultation-shortrange-e.pdf

[3] A. Ryer and V. Light, "Light measurement handbook," 1997.

[4] W. Genders, O. A., and S. Razavi, "Safety impacts of V2V communication in construction zones," in *Proc. The Annual Conference of the Canadian Society for Civil Engineering, Montreal,*, 2013.

[5] B. Schoettle and M. Flannagan, "A market-weighted description of low-beam and high-beam headlighting patterns in the US," 2011.

[6] P. Luo, Z. Ghassemlooy, H. L. Minh, E. Bentley, A. Burton, and X. Tang,

"Fundamental analysis of a car to car visible light communication system," in *2014 9th International Symposium on Communication Systems, Networks Digital Signal Processing (CSNDSP),*, July 2014, pp. 1011–1016.

[7] M. Gu, *Advanced optical imaging theory.* Springer Science & Business Media, 2000, vol. 75.

[8] European Machine Vision Association *et al.*, "EMVA standard 1288, standard for characterization of image sensors and cameras," *European Machine Vision Association Standard 1288 Release*, vol. 3, p. 29, 2010.

[9] I. Sen and D. Matolak, "Vehicle-Vehicle channel models for the 5-GHz band," *IEEE Transactions on Intelligent Transportation Systems*, vol. 9, no. 2, pp. 235–245, June 2008.

[10] Point Grey, "Flea3 USB 3.0 digital camera technical reference version 7.0," Sept. 2014.

[11] World Health Organization, "Global status report on road safety time for action," World Health Organization, Geneva, Switzerland, Tech. Rep., 2009, ISBN: 9789241563840.

[12] C. D. Mathers and D. Loncar, "Projections of global mortality and burden of disease from 2002 to 2030," *PLOS medicine*, vol. 3, no. 11, p. e442, 2006.

[13] W. J. Fleming, "New automotive sensors a review," *IEEE Sensors Journal*, vol. 8, no. 11, pp. 1900–1921, 2008.

[14] M. Pinelis, "Automotive sensors and electronics: trends and developments in

2013," *Automotive Sensors and Electronics Expo, Detroit, MI, USA*, October 2013.

[15] Google Corporation. (2015, October) Google self-driving car project monthly report. [Online]. Available: https://static.googleusercontent.com/media/www.google.com/en//selfdrivingcar/files/reports/report-1015.pdf

[16] The Volvo Group. (2015) Volvo autopilot. [Online]. Available: http://www.volvocars.com/au/about/innovations/intellisafe/autopilot

[17] Y. Kageyama. (2015, October) Toyota self-driving car goes for a spin. [Online]. Available: http://www.theglobeandmail.com/globe-drive/toyota-self-driving-car-goes-for-a-spin/article26684096/

[18] The Tesla Motors Team. Your autopilot has arrived. [Online]. Available: https://www.teslamotors.com/en_CA/blog/your-autopilot-has-arrived

[19] J. Carroll, M. Seidl, R. Cuerden, and A. Stevens, "Technical considerations regarding type-approval testing of ecall in-vehicle systems," Transport Research Laboratory, Tech. Rep., March 2014.

[20] V. Barabba, C. Huber, F. Cooke, N. Pudar, J. Smith, and M. Paich, "A multi-method approach for creating new business models: The general motors OnStar project," *Interfaces*, vol. 32, no. 1, pp. 20–34, 2002.

[21] National Highway Traffic Safety Administration, "Federal motor vehicle safety standards: Vehicle-to-vehicle (V2V) communications docket no. NHTSA20140022," August 2014.

[22] National Conference of State Legislatures. Autonomous self-driving vehicles legislation. [Online]. Available: http://www.ncsl.org/research/transportation/autonomous-vehicles-legislation.aspx

[23] Ontario Government. (2015, October) Self-driving cars to be tested on ontario roads. [Online]. Available: http://www.cbc.ca/news/canada/kitchener-waterloo/ontario-announcement-automated-cars-1.3268181

[24] A. Vahidi and A. Eskandarian, "Research advances in intelligent collision avoidance and adaptive cruise control," *IEEE Transactions on Intelligent Transportation Systems*, vol. 4, no. 3, pp. 143–153, 2003.

[25] C. Olaverri-Monreal, P. Gomes, R. Fernandes, F. Vieira, and M. Ferreira, "The see-through system: A VANET-enabled assistant for overtaking maneuvers," in *2010 IEEE Intelligent Vehicles Symposium (IV),*, June 2010, pp. 123–128.

[26] W. Chen and S. Cai, "Ad hoc peer-to-peer network architecture for vehicle safety communications," *IEEE Communications Magazine*, vol. 43, no. 4, pp. 100–107, April 2005.

[27] J. Anda, J. LeBrun, D. Ghosal, C.-N. Chuah, and M. Zhang, "VGrid: vehicular adhoc networking and computing grid for intelligent traffic control," in *2005 IEEE 61st Vehicular Technology Conference, 2005. VTC 2005-Spring.*, vol. 5, May 2005, pp. 2905–2909 Vol. 5.

[28] K. Ahn, H. Rakha, A. Trani, M. V. Aerde, and V. Aerde, "Estimating vehicle fuel consumption and emissions based on instantaneous speed and acceleration levels," *ASCE Journal of Transportation Engineering*, pp. 182–190, 2002.

[29] B. Mohandas, R. Liscano, and O. Yang, "Vehicle traffic congestion management in vehicular ad-hoc networks," in *IEEE 34th Conference on Local Computer Networks, 2009. LCN 2009.*, Oct 2009, pp. 655–660.

[30] Telefonica Digital. (2013) Connected car industry report. [Online]. Available: https://m2m.telefonica.com/system/files_force/telefonica_digital_connected_car_report_english_36.pdf

[31] A. Balasubramanian, R. Mahajan, A. Venkataramani, B. N. Levine, and J. Zahorjan, "Interactive wifi connectivity for moving vehicles," in *Proceedings of the ACM SIGCOMM 2008 Conference on Data Communication*, ser. SIGCOMM '08. New York, NY, USA: ACM, 2008, pp. 427–438. [Online]. Available: http://doi.acm.org/10.1145/1402958.1403006

[32] J. Lin, S.-C. Chen, Y.-T. Shih, and S.-H. Chen, "A study on remote on-line diagnostic system for vehicles by integrating the technology of OBD, GPS, and 3G," *Engineering and Technology World Academy of Science*, vol. 56, pp. 435–441, 2009.

[33] M. Pinelis, "Automotive sensors and electronics: trends and developments in 2013," *Automotive Sensors and Electronics Expo, Detroit, MI, USA*, October 2013.

[34] T. Zhang, H. Antunes, and S. Aggarwal, "Defending connected vehicles against malware: Challenges and a solution framework," *IEEE Internet of Things Journal*, vol. 1, no. 1, pp. 10–21, Feb 2014.

[35] J.-P. Hubaux, S. Capkun, and J. Luo, "The security and privacy of smart vehicles," *IEEE Security and Privacy*, no. 3, pp. 49–55, 2004.

[36] A. Francillon, B. Danev, S. Capkun, S. Capkun, and S. Capkun, "Relay attacks on passive keyless entry and start systems in modern cars." in *NDSS*, 2011.

[37] R. M. Ishtiaq Roufa, H. Mustafaa, S. O. Travis Taylora, W. Xua, M. Gruteserb, W. Trappeb, and I. Seskarb, "Security and privacy vulnerabilities of in-car wireless networks: A tire pressure monitoring system case study," in *19th USENIX Security Symposium, Washington DC*, 2010, pp. 11–13.

[38] C. Miller and C. Valasek. Hackers remotely kill a Jeep on the highwaywith me in it. [Online]. Available: http://www.wired.com/2015/07/hackers-remotely-kill-jeep-highway/

[39] N. Lu, N. Cheng, N. Zhang, X. Shen, and J. W. Mark, "Connected vehicles: Solutions and challenges," *IEEE Internet of Things Journal*, vol. 1, no. 4, pp. 289–299, 2014.

[40] J. Luo and J.-P. Hubaux, "A survey of inter-vehicle communication," School of Computer and Communication Sciences EPFL, CH-1015 Lausanne, Switzerland, Tech. Rep., 2004.

[41] M. Boban, T. T. Vinhoza, M. Ferreira, J. Barros, and O. K. Tonguz, "Impact of vehicles as obstacles in vehicular ad hoc networks," *IEEE Journal on Selected Areas in Communications*, vol. 29, no. 1, pp. 15–28, 2011.

[42] "IEEE standard for information technology– local and metropolitan area networks– specific requirements– part 11: Wireless LAN medium access control

(MAC) and physical layer (PHY) specifications amendment 6: Wireless access in vehicular environments," *IEEE Std 802.11p-2010 (Amendment to IEEE Std 802.11-2007 as amended by IEEE Std 802.11k-2008, IEEE Std 802.11r-2008, IEEE Std 802.11y-2008, IEEE Std 802.11n-2009, and IEEE Std 802.11w-2009)*, pp. 1–51, July 2010.

[43] "IEEE draft guide for wireless access in vehicular environments (WAVE) - architecture," *IEEE P1609.0/D5, September 2012*, pp. 1–74, Oct 2012.

[44] L. Cheng, B. Henty, D. Stancil, F. Bai, and P. Mudalige, "Mobile vehicle-to-vehicle narrow-band channel measurement and characterization of the 5.9 GHz dedicated short range communication (DSRC) frequency band," *IEEE Journal on Selected Areas in Communications,*, vol. 25, no. 8, pp. 1501–1516, Oct 2007.

[45] F. Yu and S. Biswas, "Self-configuring TDMA protocols for enhancing vehicle safety with DSRC based vehicle-to-vehicle communications," *IEEE Journal on Selected Areas in Communications,*, vol. 25, no. 8, pp. 1526–1537, Oct 2007.

[46] J. S. Davis, J.-P. P. Linnartz *et al.*, "Vehicle to vehicle RF propagation measurements," in *1994 Conference Record of the Twenty-Eighth Asilomar Conference on Signals, Systems and Computers, 1994.*, vol. 1. IEEE, 1994, pp. 470–474.

[47] G. Acosta, K. Tokuda, and M. A. Ingram, "Measured joint doppler-delay power profiles for vehicle-to-vehicle communications at 2.4 GHz," in *IEEE Global Telecommunications Conference, 2004. GLOBECOM'04.*, vol. 6. IEEE, 2004, pp. 3813–3817.

[48] W. Viriyasitavat, M. Boban, H.-M. Tsai, and A. Vasilakos, "Vehicular communications: Survey and challenges of channel and propagation models," *IEEE Vehicular Technology Magazine*, vol. 10, no. 2, pp. 55–66, 2015.

[49] D. Matolak, I. Sen, W. Xiong, and R. Apaza, "Channel measurement/modeling for airport surface communications: Mobile and fixed platform results," *IEEE Aerospace and Electronic Systems Magazine,*, vol. 22, no. 10, pp. 25–30, Oct 2007.

[50] D. Matolak, I. Sen, and W. Xiong, "Channel modeling for V2V communications," in *2006 Third Annual International Conference on Mobile and Ubiquitous Systems: Networking Services,*, July 2006, pp. 1–7.

[51] G. Acosta-Marum and M. Ingram, "Doubly selective vehicle-to-vehicle channel measurements and modeling at 5.9 GHz," in *Proc. Int. Symp. Wireless Personal Multimedia Commun.* Citeseer, 2006.

[52] F. Vatalaro and A. Forcella, "Doppler spectrum in mobile-to-mobile communications in the presence of three-dimensional multipath scattering," *IEEE Transactions on Vehicular Technology,*, vol. 46, no. 1, pp. 213–219, 1997.

[53] F. Bai and H. Krishnan, "Reliability analysis of DSRC wireless communication for vehicle safety applications," in *IEEE Intelligent Transportation Systems Conference, 2006. ITSC '06.*, 2006, pp. 355–362.

[54] C.-N. Liang and B.-C. Chen, "A study of DSRC jammer in vehicle safety application testbed," in *2012 12th International Conference on ITS Telecommunications (ITST)*, 2012, pp. 216–219.

[55] D. Jiang, V. Taliwal, A. Meier, W. Holfelder, and R. Herrtwich, "Design of 5.9 GHz DSRC-based vehicular safety communication," *IEEE Wireless Communications*, vol. 13, no. 5, pp. 36–43, 2006.

[56] S. Biswas, R. Tatchikou, and F. Dion, "Vehicle-to-vehicle wireless communication protocols for enhancing highway traffic safety," *IEEE Communications Magazine*, vol. 44, no. 1, pp. 74–82, 2006.

[57] J. Yin, T. ElBatt, G. Yeung, B. Ryu, S. Habermas, H. Krishnan, and T. Talty, "Performance evaluation of safety applications over DSRC vehicular ad hoc networks," in *Proceedings of the 1st ACM International Workshop on Vehicular Ad Hoc Networks*, ser. VANET '04. New York, NY, USA: ACM, 2004, pp. 1–9. [Online]. Available: http://doi.acm.org/10.1145/1023875.1023877

[58] Q. Xu, T. Mak, J. Ko, and R. Sengupta, "Vehicle-to-vehicle safety messaging in DSRC," in *Proceedings of the 1st ACM International workshop on Vehicular ad hoc networks*. ACM, 2004, pp. 19–28.

[59] S. Bharati and W. Zhuang, "CAH-MAC: Cooperative ADHOC MAC for vehicular networks," *IEEE Journal on Selected Areas in Communications,*, vol. 31, no. 9, pp. 470–479, September 2013.

[60] International Telecommunications Union, "Recommendation m.1677-1, international morse code," *ITU*, 2009.

[61] D. Steigerwald, J. Bhat, D. Collins, R. M. Fletcher, M. Holcomb, M. Ludowise, P. Martin, and S. Rudaz, "Illumination with solid state lighting technology,"

IEEE Journal of Selected Topics in Quantum Electronics, vol. 8, no. 2, pp. 310–320, Mar 2002.

[62] OMEGA, "Project home gigabit access. European Commission," May 2015. [Online]. Available: http://www.ict-omega.eu/

[63] S. Rajagopal, R. Roberts, and S.-K. Lim, "IEEE 802.15.7 visible light communication: modulation schemes and dimming support," *IEEE Communications Magazine,*, vol. 50, no. 3, pp. 72–82, March 2012.

[64] A. Wilkins, J. Veitch, and B. Lehman, "LED lighting flicker and potential health concerns: IEEE standard PAR1789 update," in *2010 IEEE Energy Conversion Congress and Exposition (ECCE)*, Sept 2010, pp. 171–178.

[65] "Visible light communication system standard," JEITA CP-1221, 2007.

[66] "Visible light ID system standard," JEITA CP-1222, 2007.

[67] D. Steigerwald, J. C. Bhat, D. Collins, R. M. Fletcher, M. O. Holcomb, M. J. Ludowise, P. S. Martin, S. L. Rudaz *et al.*, "Illumination with solid state lighting technology," *IEEE Journal of Selected Topics in Quantum Electronics,*, vol. 8, no. 2, pp. 310–320, 2002.

[68] J. Grubor, S. Randel, K.-D. Langer, and J. Walewski, "Broadband information broadcasting using led-based interior lighting," *Journal of Lightwave Technology,*, vol. 26, no. 24, pp. 3883–3892, Dec 2008.

[69] D. C. O'Brien, L. Zeng, H. Le-Minh, G. Faulkner, J. W. Walewski, and S. Randel, "Visible light communications: Challenges and possibilities," in *IEEE 19th*

International Symposium on Personal, Indoor and Mobile Radio Communications, 2008. PIMRC 2008. IEEE, 2008, pp. 1–5.

[70] E. Monteiro and S. Hranilovic, "Design and implementation of color-shift keying for visible light communications," *Journal of Lightwave Technology,*, vol. 32, no. 10, pp. 2053–2060, 2014.

[71] "IEEE standard for local and metropolitan area networks–Part 15.7: Short-range wireless optical communication using visible light," *IEEE Std 802.15.7-2011*, pp. 1–309, Sept 2011.

[72] P. Butala, J. Chau, and T. Little, "Metameric modulation for diffuse visible light communications with constant ambient lighting," in *2012 International Workshop on Optical Wireless Communications (IWOW),*, Oct 2012, pp. 1–3.

[73] IEEE Standards Association *et al.*, "IEEE 802.15TM: Wireless personal area networks (PANs)."

[74] Byte Light, "Indoor location based software. Byte Light," May 2015. [Online]. Available: http://www.bytelight.com/

[75] Visible Light Communication Consortium, "Home Visible Light Communication Consortium," May 2015. [Online]. Available: http://www.vlcc.net

[76] S. Landau and J. Erion, "Automotive: Car makers embrace led signals," *Nature Photonics*, vol. 1, no. 1, pp. 31–32, 2007.

[77] W. Viriyasitavat, S.-H. Yu, and H.-M. Tsai, "Short paper: Channel model for visible light communications using off-the-shelf scooter taillight," in *2013 IEEE Vehicular Networking Conference (VNC),*. IEEE, 2013, pp. 170–173.

[78] S.-H. Yu, O. Shih, H.-M. Tsai, and R. Roberts, "Smart automotive lighting for vehicle safety," *IEEE Communications Magazine*, vol. 51, no. 12, pp. 50–59, December 2013.

[79] C. B. Liu, B. Sadeghi, and E. W. Knightly, "Enabling vehicular visible light communication (V2LC) networks," in *Proceedings of the Eighth ACM international workshop on Vehicular inter-networking*. ACM, 2011, pp. 41–50.

[80] R. Roberts, P. Gopalakrishnan, and S. Rathi, "Visible light positioning: automotive use case," in *2010 IEEE Vehicular Networking Conference (VNC)*. IEEE, 2010, pp. 309–314.

[81] N. Kumar, D. Terra, N. Lourenco, L. Alves, and R. L. Aguiar, "Visible light communication for intelligent transportation in road safety applications," in *2011 7th International Wireless Communications and Mobile Computing Conference (IWCMC)*, 2011, pp. 1513–1518.

[82] I. E. Lee, M. L. Sim, and F. W. L. Kung, "A dual-receiving visible-light communication system for intelligent transportation system," in *4th IEEE International Conference on Circuits and Systems for Communications, 2008. ICCSC 2008*, 2008, pp. 698–702.

[83] T. Hara, S. Iwasaki, T. Yendo, T. Fujii, and M. Tanimoto, "A new receiving system of visible light communication for ITS," in *2007 IEEE Intelligent Vehicles Symposium*, 2007, pp. 474–479.

[84] S. Okada, T. Yendo, T. Yamazato, T. Fujii, M. Tanimoto, and Y. Kimura,

"On-vehicle receiver for distant visible light road-to-vehicle communication," in *2009 IEEE Intelligent Vehicles Symposium*, 2009, pp. 1033–1038.

[85] Y. Yi, P. Li, C. Li, and C. Azurdia, "An effective scheme for optical doppler shift alleviation in intelligent transportation system integrating visible light communication," in *2011 13th International Conference on Advanced Communication Technology (ICACT)*, 2011, pp. 1253–1258.

[86] K. Cui, G. Chen, Z. Xu, and R. Roberts, "Experimental characterization of traffic light to vehicle VLC link performance," in *2011 IEEE GLOBECOM Workshops (GC Wkshps)*, 2011, pp. 808–812.

[87] J. Liu, P. Chan, D. Ng, E. Lo, and S. Shimamoto, "Hybrid visible light communications in intelligent transportation systems with position based services," in *2012 IEEE Globecom Workshops (GC Wkshps)*, 2012, pp. 1254–1259.

[88] D.-R. Kim, S.-H. Yang, H.-S. Kim, Y.-H. Son, and S.-K. Han, "Outdoor visible light communication for inter-vehicle communication using controller area network," in *2012 Fourth International Conference on Communications and Electronics (ICCE)*, 2012, pp. 31–34.

[89] N. Naylor, "NHTSA announces final rule requiring rear visibility technology," March 2014. [Online]. Available: www.dmg.utoronto.ca/pdf/tts/2011/2011od_report_full.pdf

[90] Mini, "Mini connected, GOPRO ready." June 2014. [Online]. Available: www.MINIUSA.com/Connected

[91] R. Massey and V. Woollaston. (2015, June) Ford's cars can now see round corners: Split-view camera warns of obstacles even on blind junctions. [Online]. Available: http://www.dailymail.co.uk/sciencetech/article-3135933/Ford-s-cars-round-CORNERS-Split-view-camera-warns-obstacles-blind-junctions.html

[92] R. Roberts, "Project: IEEE P802.15 working group for wireless personal area networks (WPANs),on study group status for camera communications," *IEEE P802.15*, July 2013.

[93] H. Premachandra, T. Yendo, M. Tehrani, T. Yamazato, H. Okada, T. Fujii, and M. Tanimoto, "High-speed-camera image processing based LED traffic light detection for road-to-vehicle visible light communication," in *2010 IEEE Intelligent Vehicles Symposium (IV)*, 2010, pp. 793–798.

[94] D.-R. Kim, S.-H. Yang, H.-S. Kim, Y.-H. Son, and S.-K. Han, "Outdoor visible light communication for inter- vehicle communication using controller area network," in *2012 Fourth International Conference on Communications and Electronics (ICCE),*, Aug 2012, pp. 31–34.

[95] N. Kumar, N. Lourenco, D. Terra, L. Alves, and R. L. Aguiar, "Visible light communications in intelligent transportation systems," in *Intelligent Vehicles Symposium (IV), 2012 IEEE*, June 2012, pp. 748–753.

[96] H. Premachandra, T. Yendo, M. Tehrani, T. Yamazato, H. Okada, T. Fujii, and M. Tanimoto, "High-speed-camera image processing based LED traffic light detection for road-to-vehicle visible light communication," in *2010 IEEE Intelligent Vehicles Symposium (IV),*, June 2010, pp. 793–798.

[97] S. Iwasaki, C. Premachandra, T. Endo, T. Fujii, M. Tanimoto, and Y. Kimura, "Visible light road-to-vehicle communication using high-speed camera," in *2008 IEEE Intelligent Vehicles Symposium,*, June 2008, pp. 13–18.

[98] L. Zeng, D. C. O'Brien, H. Minh, G. E. Faulkner, K. Lee, D. Jung, Y. Oh, and E. T. Won, "High data rate multiple input multiple output (MIMO) optical wireless communications using white LED lighting," *IEEE Journal on Selected Areas in Communications*, vol. 27, no. 9, pp. 1654–1662, December 2009.

[99] A. Ashok, M. Gruteser, N. Mandayam, J. Silva, M. Varga, and K. Dana, "Challenge: Mobile optical networks through visual MIMO," in *Proceedings of the Sixteenth Annual International Conference on Mobile computing and networking*. ACM, 2010, pp. 105–112.

[100] P. Ji, H.-M. Tsai, C. Wang, and F. Liu, "Vehicular visible light communications with LED taillight and rolling shutter camera," in *Vehicular Technology Conference (VTC Spring), 2014 IEEE 79th*, May 2014, pp. 1–6.

[101] R. Roberts, "Undersampled frequency shift ON-OFF keying (UFSOOK) for camera communications (CamCom)," in *2013 22nd Wireless and Optical Communication Conference (WOCC),*, May 2013, pp. 645–648.

[102] I. Takai, T. Harada, M. Andoh, K. Yasutomi, K. Kagawa, and S. Kawahito, "Optical vehicle-to-vehicle communication system using led transmitter and camera receiver," *IEEE Photonics Journal,*, vol. 6, no. 5, pp. 1–14, Oct 2014.

[103] T. Yamazato, I. Takai, H. Okada, T. Fujii, T. Yendo, S. Arai, M. Andoh, T. Harada, K. Yasutomi, K. Kagawa, and S. Kawahito, "Image-sensor-based

visible light communication for automotive applications," *IEEE Communications Magazine,*, vol. 52, no. 7, pp. 88–97, July 2014.

[104] W. Genders, "A microsimulation approach assessing the impact of connected vehicle on work zone traffic safety," Master's thesis, McMaster University, 2014.

[105] P. G. Angott, "Remotely controlled ceiling fan and light assembly," Nov. 11 1986, US Patent 4,621,992.

[106] H. T. Friis, "A note on a simple transmission formula," *IRE proc.*, vol. 34, no. 5, pp. 254–256, 1946.

[107] T. S. Rappaport *et al.*, *Wireless communications: principles and practice.* prentice hall PTR New Jersey, 1996, vol. 2.

[108] J. W. Byers, M. Luby, M. Mitzenmacher, and A. Rege, "A digital fountain approach to reliable distribution of bulk data," in *ACM SIGCOMM Computer Communication Review*, vol. 28, no. 4. ACM, 1998, pp. 56–67.

[109] A. Shokrollahi, "Raptor codes," *IEEE Transactions on Information Theory*, vol. 52, no. 6, pp. 2551–2567, 2006.

[110] M. Luby, "LT codes," in *Proceedings of the 43rd Symposium on Foundations of Computer Science*, ser. FOCS '02. Washington, DC, USA: IEEE Computer Society, 2002, p. 271. [Online]. Available: http://dl.acm.org/citation.cfm?id=645413.652135

[111] T. Truong, I. Hsu, W. Eastman, and I. Reed, "Simplified procedure for correcting both errors and erasures of reed-solomon code using euclidean algorithm,"

IEEE Proceedings Computers and Digital Techniques, vol. 135, no. 6, pp. 318–324, 1988.

[112] J.-H. Jeng and T.-K. Truong, "On decoding of both errors and erasures of a Reed-Solomon code using an inverse-free Berlekamp-Massey algorithm," *IEEE Transactions on Communications,*, vol. 47, no. 10, pp. 1488–1494, 1999.

[113] W. C. Huffman and V. Pless, *Fundamentals of error-correcting codes.* Cambridge university press, 2003.

[114] ISO 11664 / CIE S 014. (2013, March) Cie: International commission on illumination. [Online]. Available: http://www.cie.co.at/index.php/Publications/Standards

[115] "Rolling Shutter vs. Global Shutter Technical Note," http://www.qimaging.com/ccdorscmos/pdfs/RollingvsGlobalShutter.pdf, 2014.

[116] C.-K. Liang, L.-W. Chang, and H. H. Chen, "Analysis and compensation of rolling shutter effect," *IEEE Transactions on Image Processing*, vol. 17, no. 8, pp. 1323–1330, 2008.

[117] B. Jähne, *Digital image processing, 1st ed. (1991) - 6th ed. (2005).* Springer, 2005.

[118] R. Klette, K. Schlüns, and A. Koschan, *Computer vision: three-dimensional data from images.* Springer Singapore, 1998, vol. 1.

[119] National Highway Traffic Safety Administration, "Traffic safety facts 2012: A compilation of motor vehicle crash data from the fatality analysis reporting

system and the general estimates system," United States Department of Transportation, Tech. Rep. DOT HS 812 032, 2014.

[120] The European Telecommunications Standards Institute, "Electromagnetic compatibility and radio spectrum matters (ERM) intelligent transport systems (ITS) Part 1: Technical characteristics for pan-european harmonized communications equipment operating in the 5 GHz frequency range and intended for critical road-safety applications system reference document," in *ETSI TR 102 492-1 V1.1.1*, june 2005.

[121] F. Capulli, C. Monti, M. Vari, and F. Mazzenga, "Path loss models for ieee 802.11a wireless local area networks," in *3rd International Symposium on Wireless Communication Systems, 2006. ISWCS '06.*, Sept 2006, pp. 621–624.

[122] Y. J. Li, "An overview of the dsrc/wave technology," in *Quality, Reliability, Security and Robustness in Heterogeneous Networks.* Springer, 2010, pp. 544–558.

[123] University of Michigan's Mobility Transformation Center. University of michigan's cityscape will test driverless vehicles. [Online]. Available: http://ns.umich.edu/new/multimedia/videos/22608-u-m-s-cityscape-will-test-driverless-vehicles

[124] Quadstone Paramics, "Paramics v. 6.9.3." [Online]. Available: www.paramics-online.com/

[125] C. Bachmann, M. J. Roorda, and B. Abdulhai, "Simulating traffic conflicts on truck-only infrastructure using an improved time to collision definition,"

in *Transportation Research Board Meeting, Washington, DC: Transportation Research Board*, 2010.

[126] Data management Group, University of Toronto, "Transportation tomorrow 2011 survey area summary 2011, 2006, 2001, 1996, 1986 origin-destination matrices." [Online]. Available: www.dmg.utoronto.ca/pdf/tts/2011/2011od_report_full.pdf

[127] S. G. Klauer, T. A. Dingus, V. L. Neale, J. D. Sudweeks, and D. J. Ramsey, "The impact of driver inattention on near-crash/crash risk: An analysis using the 100-car naturalistic driving study data," Tech. Rep. DOT HS 810 594, 2006.

[128] R. Kiefer, D. LeBlanc, M. Palmer, J. Salinger, R. Deering, and M. Shulman, "Development and validation of functional definitions and evaluation procedures for collision warning/avoidance systems," Tech. Rep., 1999.

[129] C. Bennett, "Modelling driver acceleration and deceleration behaviour in New Zealand," *ND Lea International, Vancouver*, 1994.

[130] A. K. Maurya and P. S. Bokare, "Study of deceleration behaviour of different vehicle types," *International Journal for Traffic and Transport Engineering*, vol. 2, no. 3, pp. 253–270, 2012.

[131] D. K. Borah, A. C. Boucouvalas, C. C. Davis, S. Hranilovic, and K. Yiannopoulos, "A review of communication-oriented optical wireless systems," *EURASIP Journal on Wireless Communications and Networking*, pp. 1–28, 2012.

[132] B. Schoettle, M. Sivak, and Y. Fujiyama, "LEDs and power consumption of

exterior automotive lighting: implications for gasoline and electric vehicles," 2008.

[133] J. Barry, J. Kahn, W. Krause, E. Lee, and D. Messerschmitt, "Simulation of multipath impulse response for indoor wireless optical channels," *IEEE Journal on Selected Areas in Communications,*, vol. 11, no. 3, pp. 367–379, Apr 1993.

[134] American Concrete Pavement Association, "Albedo: A measure of pavement surface reflectance," *IEEE Journal on Selected Areas in Communications,*, no. 3.05, June 2002.

[135] T. Komine and M. Nakagawa, "Fundamental analysis for visible-light communication system using LED lights," *IEEE Transactions on Consumer Electronics,*, vol. 50, no. 1, pp. 100–107, Feb 2004.

[136] R. Nebuloni and C. Capsoni, "Laser attenuation by falling snow," in *6th International Symposium on Communication Systems, Networks and Digital Signal Processing, 2008. CNSDSP 2008.*, July 2008, pp. 265–269.

[137] M. S. Awan, L. C. Horwath, S. S. Muhammad, E. Leitgeb, F. Nadeem, and M. S. Khan, "Characterization of fog and snow attenuations for free-space optical propagation," *Journal of Communications*, vol. 4, no. 8, pp. 533–545, Sep 2009.

[138] J. Kahn and J. Barry, "Wireless infrared communications," *Proceedings of the IEEE*, vol. 85, no. 2, pp. 265–298, Feb 1997.

[139] Linear Technology, "500mA power op amp with adjustable precision current limit," LT1970A.

[140] A. Cailean, B. Cagneau, L. Chassagne, S. Topsu, Y. Alayli, and J.-M. Blosseville, "Visible light communications: Application to cooperation between vehicles and road infrastructures," in *2012 IEEE Intelligent Vehicles Symposium (IV),*. IEEE, 2012, pp. 1055–1059.

[141] S. Schmid, G. Corbellini, S. Mangold, and T. R. Gross, "LED-to-LED visible light communication networks," in *Proceedings of the fourteenth ACM international symposium on Mobile ad hoc networking and computing*. ACM, 2013, pp. 1–10.

[142] J. R. Meyer-Arendt, "Radiometry and photometry: Units and conversion factors," *Applied Optics*, vol. 7, no. 10, pp. 2081–2084, 1968.

[143] C. W. Gardiner *et al.*, *Handbook of stochastic methods*. Springer Berlin, 1985, vol. 4.

[144] B. E. Saleh, M. C. Teich, and B. E. Saleh, *Fundamentals of photonics*. Wiley New York, 1991, vol. 22.

[145] P. Viola and M. Jones, "Rapid object detection using a boosted cascade of simple features," in *Proceedings of the 2001 IEEE Computer Society Conference on Computer Vision and Pattern Recognition, 2001. CVPR 2001.*, vol. 1. IEEE, 2001, pp. I–511.